Inhibition of Notch activity by phosphorylation of CSL in response to parasitization in *Drosophila*

*Sebastian Deichsel[1,#], Lisa Frankenreiter[1], Johannes Fechner[1,§], Bernd M. Gahr[1,+], Mirjam Zimmermann[1], Helena Mastel[1], Irina Preis[1], Anette Preiss[1,&], Anja C. Nagel[1]**

Department of Molecular Genetics, Institute of Biology, University of Hohenheim, 70599 Stuttgart, Germany

now at: Department of Medical Genetics and Applied Genomics, University of Tübingen, 72076 Tübingen, Germany

§ now at: Institute of Biomedical Genetics (IBMG), University of Stuttgart, 70569 Stuttgart, Germany

+ now at: Department of Internal Medicine II, Molecular Cardiology, University of Ulm, 89081 Ulm, Germany

& emerita professor

* Author for correspondence: anja.nagel@uni-hohenheim.de

Key words

CSL, *Drosophila melanogaster*, host defense, immune challenge, Notch inhibition, parasitoid wasp, phosphorylation, PKC, Suppressor of Hairless.

Declaration of interests

The authors declare that no competing interests exist.

Abstract

Notch signaling activity regulates hematopoiesis in *Drosophila* and vertebrates alike. Parasitoid wasp infestation of *Drosophila* larvae, however, requires a rapid downregulation of Notch activity to allow the formation of encapsulation-active blood cells. Here we show that the *Drosophila* CSL transcription factor Suppressor of Hairless [Su(H)] is phosphorylated at Serine 269 in response to parasitoid wasp infestation. As this phosphorylation interferes with the DNA-binding of Su(H), it reversibly inhibits Notch activity. Accordingly, phospho-deficient $Su(H)^{S269A}$ mutants are immune compromised. A screen for kinases involved in Su(H) phosphorylation identified Pkc53E, required for normal hematopoiesis as well as for parasitoid immune response. Genetic and molecular interactions support the specificity of the Su(H)-Pkc53E relationship. Moreover, phorbol ester treatment inhibits Su(H) activity in vivo and in human cell culture. We conclude that Pkc53E targets Su(H) during parasitic wasp infestation, inducing downregulation of Notch activity, thereby remodeling the blood cell population required for wasp egg encapsulation.

Introduction

Drosophila melanogaster harbours a sophisticated cellular immune system to fight invaders. The larval hematopoietic system comprises a circulating and sessile compartment of embryonic origin and the developing larval lymph gland, constituting a hematopietic organ. The circulating and sessile compartment consists primarily of macrophage-like plasmatocytes, plus a small number of crystal cells involved in wound healing and melanization responses to neutralize pathogens. Both cell types differentiate from hemocyte precursors within the lymph gland as well; they are released during pupal stages to serve the adult with immune cells. Finally, lamellocytes represent the third blood cell type in *Drosophila*. While merely absent in healthy animals, their formation is induced within hours of wasp infestation or wounding (reviewed in: Banerjee et al., 2019; Letourneau et al., 2016; Hultmark and Andó, 2022). In fact, parasitism by endo-parasitoid wasps represents one of the most severe naturally occurring immune challenges to *Drosophila*, invariably causing death if not defended off properly. Parasitoid wasps deposit their egg into the live *Drosophila* larva, where it develops into the next wasp generation egressing from the pupa instead of a fly. Hence, wasp infestation is a life-threatening challenge to the *Drosophila* host, demanding an immediate immune response to overwhelm the parasite. This involves a massive increase in circulating hemocytes, and most energy resources are devoted to fight the invader. Here, lamellocytes play a critical role: they encapsulate the wasp egg and, by expressing Prophenoloxidase, induce a melanization reaction retarding further wasp development (Dudzic et al. 2015; reviewed in: Banerjee et al., 2019; Letourneau et al., 2016; Hultmark and Andó, 2022).

Wasp infestation dramatically remodels the composition of the *Drosophila* hemocyte population (Cho et al., 2020; Tattikota et al., 2020; reviewed in: Csordás et al., 2021). There is a vast increase in plasmatocytes and intermediate precursors in both hematopoietic compartments, from which lamellocyte differentiate, requiring the combined activity of several pathways, including JAK/STAT, JNK, Toll, Notch, EGFR and INR pathways, which in fact regulate blood cell homeostasis in general (reviewed in Banerjee et al., 2019; Letournau et al., 2018; Csordás et al., 2021). Simultaneous to the massive expansion of lamellocytes, crystal cells derived from the same precursors are significantly reduced (Crozatier et al., 2004; Krzemien et al., 2010; Ferguson and Martinez –Agosto, 2014; Cho et al., 2020; Tattikota et al., 2020; reviewed in Csordás et al., 2021). Crystal cells are generated both in the larval lymph gland as well as by trans-differentiation from plasmatocytes in the sessile compartment. Their formation, differentiation and survival strictly depend on Notch signaling activity (reviewed in: Banerjee et al., 2019; Csordás et al., 2021; Hultmark and Andó, 2022). Lamellocyte and crystal

cell lineages are mutually exclusive. Accordingly, while promoting crystal cell fate, Notch activity inhibits differentiation of lamellocytes within the lymph gland, however, is reduced upon wasp infestation (Small et al., 2014). Lamellocyte induction involves the formation and sensing of reactive oxygen species triggered by wasp egg injection (Nappi et al., 1995; Sinenko et al., 2011; Small et al., 2014; Louradour et al., 2017; reviewed in: Banerjee et al., 2019; Csordás et al., 2021). The molecular mechanism underlying the simultaneous crystal cell fate inhibition, however, is less well understood. Obviously, an effective and rapid downregulation of Notch activity is required to fend off parasitic wasps.

The Notch pathway is highly conserved between invertebrates and vertebrates, where it regulates numerous cell fate decisions. Notch signals are transduced by CSL type proteins (abbreviation of human CBF1/RBPJ, *Drosophila* Suppressor of Hairless [Su(H)], and worm Lag1), that bind the DNA to direct transcriptional activity of Notch target genes by help of recruited cofactors (reviewed in: Giaimo et al., 2021; Kopan and Ilagan, 2009; Siebel and Lendahl, 2017). Hence, CSL is central to Notch pathway activity as no signal transduction could occur in its absence or in the instance of a lack of DNA-binding. Earlier, we observed CSL, i.e. Su(H) phosphorylation at Serine 269 in cultured *Drosophila* Schneider S2 cells (Nagel et al., 2017). Of note, Schneider S2 cells have hemocyte characteristics (Cherbas et al., 2011; Schneider, 1972; Terriente-Felix et al., 2013). As a consequence of the negative charge conferred by the phosphorylation at Serine 269, Su(H) loses its affinity to the DNA, and without its DNA-binding ability, also its function as a transcriptional regulator (Nagel et al., 2017). Accordingly, a phospho-mimetic $Su(H)^{S269D}$ mutant behaved like a *Su(H)* loss of function mutant in all respects. In contrast, the phospho-deficient $Su(H)^{S269A}$ variant, appeared wild type at the first glance, indicating some tissue-specificity of this regulatory mechanism. In fact, the $Su(H)^{S269A}$ allele displayed a gain of Notch activity particularly during embryonic and larval hematopoiesis with increased numbers of crystal cells in both hematopoietic compartments (Frankenreiter et al., 2021). Moreover, we found that the general Notch antagonist Hairless is not involved in constraining crystal cell numbers, suggesting that in the context of blood cell homeostasis Notch activity is regulated by the phosphorylation of Su(H) (Maier, 2006; Frankenreiter et al., 2021). As the same set of genes affect blood cell maintenance and differentiation in homeostasis and upon immune challenge (Cho et al., 2020; Tattikota et al., 2020), obviously phospho-mediated downregulation of Notch activity might also occur in response to parasitoid wasp infestation, allowing the formation of encapsulation active lamellocytes at the expense of crystal cells. Briefly, phosphorylation of Su(H) is an elegant mechanism to promptly and transiently curb Notch activity.

83 In this work, we followed the tempting hypothesis that following wasp infestation, a specific
84 kinase might be activated to phosphorylate Su(H) thereby blocking Notch activity. In this case,
85 the phospho-deficient *Su(H)*^{S269A} allele should be immune-compromised, as it cannot respond
86 to phosphorylation, i.e. remaining active even upon infection. Indeed, *Su(H)*^{S269A} displayed an
87 increased sensitivity towards parasitoid wasp infestation accompanied by an increase of crystal
88 cells at the expense of lamellocytes. Accordingly, phosphorylation of Su(H) protein was
89 detected in infested wild type larvae but not in the *Su(H)*^{S269A} mutant. In a screen for kinases
90 regulating this process, Pkc53E, the homologue of human PKCα, was identified as an important
91 player. In agreement with a role in blood cell homeostasis, a *Pkc53E*$^{\Delta 28}$ null mutant displayed
92 increased crystal cell numbers. Moreover, genetic and molecular interactions between Su(H)
93 and Pkc53E support the specificity of their relationship. Finally, *Pkc53E*$^{\Delta 28}$ was impaired in its
94 immune response to wasp infestation as well. Together, these data show that Su(H) is a target
95 of Pkc53E during parasitic wasp infestation, inducing phosphorylation and subsequent
96 downregulation of Notch activity to allow the mass production of lamellocytes required for
97 wasp defense.

98 **Results**

99

100 ***Impaired immune response to parasitoid wasps in the phospho-deficient Su(H)^{S269A} mutant***

101 Wasp infestation alters the course of hematopoiesis, as lamellocyte differentiation is massively
102 increased at the expense of crystal cells. This process requires a rapid downregulation of Notch
103 activity that may be implemented by the phosphorylation of Su(H) at Serine 269 (S269). To
104 test this model, we exposed control larvae and larvae of the phospho-deficient *Su(H)^{S269A}*
105 variant to the parasitoid wasp *Leptopilina boulardi* (*L. boulardi*) and analysed the consequences
106 on blood cell homeostasis two days post-infection. To exclude any influence of the engineered
107 genomic background, we used *Su(H)^{gwt}* for the comparison, carrying a genomic wild type
108 construct in place of the mutant (Praxenthaler et al., 2017; Frankenreiter et al., 2021).

109 Earlier we noted an excess of crystal cells in the phospho-deficient *Su(H)^{S269A}* allele, which we
110 interpret as a gain of Notch activity in consequence of the inability to be downregulated by
111 Su(H) phosphorylation (Frankenreiter et al., 2021) (Fig. 1A,B). In response to wasp
112 infestations, however, crystal cell numbers should drop to allow formation of lamellocytes
113 (Small et al., 2014; Csordás et al., 2021). Indeed in the *Su(H)^{gwt}* control, both the sessile crystal
114 cells as well as those within the larval lymph glands were significantly lessened in response to
115 wasp infestation (Fig. 1A,B). In contrast, the higher crystal cell numbers in the *Su(H)^{S269A}*
116 mutant larvae dropped to control-level only, demonstrating the inability of the mutant to detect
117 this immune challenge or to respond to it (Fig. 1A,B).

118 Increased abundance of lamellocytes upon wasp infestation was monitored *in vivo* in larval
119 hemolymph and lymph glands, using either the L1-*atilla*-GFP reporter (Honti et al., 2009) or
120 *PPO3*-Gal4::UAS-GFP (Dudzic et al., 2015), respectively. In the harvested larval hemolymph
121 of the infested *Su(H)^{gwt}* control, the hemocytes contained about 15% *PPO3*- and 23% *atilla*-
122 labelled lamellocytes (Fig. 1C,D). These numbers were significantly lower in the wasp infested
123 *Su(H)^{S269A}* larvae (Fig. C,D). Consistently, both lamellocyte reporters were robustly induced in
124 the lymph glands of the infested control, but rarely in glands of the *Su(H)^{S269A}* mutant (Fig.
125 1E,F). Obviously, the *Su(H)^{S269A}* mutant barely responds to the immune challenge raised by the
126 parasitic wasp infestation. Overall, these data support the model that S269 in Su(H) is a
127 molecular target for a kinase, phosphorylated upon immune challenge to downregulate Notch
128 activity, thereby allowing lamellocyte formation at the expense of crystal cells.

129

130 ***The phospho-deficient Su(H)^{S269A} allele cannot combat wasp infestation***

131 Parasitoid wasp infestation constitutes an extreme immune challenge for the *Drosophila* larva:
132 if not combatted by the immune system, a wasp egg, which is deposited in the larval body
133 cavity, will develop into an adult wasp, thereby killing the larval host during pupal stage.
134 Indeed, depending on the wasp species used, we measured a high mortality rate with less than
135 5% up to about 15% of surviving flies (Fig. 2A). According to our working hypothesis, the
136 phospho-deficient $Su(H)^{S269A}$ variant should not be able to properly respond to the immune
137 challenge. To test this directly, we measured the survival of $Su(H)^{S269A}$ animals upon wasp
138 infestation compared to the wild type control.
139 The two closely related wasp species *L. boulardi* and *Leptopilina heterotoma* (*L. heterotoma*)
140 very efficiently parasitized both the control $Su(H)^{gwt}$ and the $Su(H)^{S269A}$ variant, though the latter
141 appeared slightly more sensitive (Fig. 2A). The difference in mortality became more apparent
142 with the wasp species *Asobara japonica* (*A. japonica*), allowing 14.5% of the $Su(H)^{gwt}$ control
143 flies to escape parasitism, whereas only 3.8% of the infested $Su(H)^{S269A}$ pupae emerged as flies.
144 Thus, the $Su(H)^{S269A}$ mutants are less robust in resisting parasitoid wasp infestation consistent
145 with a defective immune response.
146
147 ***Serine 269 of Su(H) is phosphorylated upon wasp infestation***
148 Next, we wanted to directly monitor Su(H) phosphorylation at S269 in response to wasp
149 infestation. To this end, polyclonal antibodies directed against a phosphorylated peptide
150 containing the sequence motif NRLRpSQTVSTRYLHVE were generated (α-pS269).
151 Specificity was first tested by Western blot analysis using bacterially expressed GST fusion
152 proteins containing the entire beta-trefoil domain (BTD) of Su(H), as well as with phospho-
153 mimetic (S269D) and phospho-mutant (S269A) versions. All three variants were detected by
154 the antisera. The S269D version, however, was strongly preferred, indicating that this antibody
155 does preferably recognize phospho-S269 Su(H) protein (Fig. 2 - figure supplement 1).
156 Encouraged by this result, we used this antiserum on protein extracts derived from larvae
157 infested and not infested by *L. boudardi*. For this experiment we used genome engineered fly
158 strains expressing mCherry-tagged Su(H) proteins, $Su(H)^{S269A\text{-}mCh}$ and $Su(H)^{gwt\text{-}mCh}$ for control
159 (Praxenthaler et al., 2017). Su(H) proteins were trapped using RFP-nanobody coupled agarose
160 beads, and the precipitates were then probed in Western blots with antibodies directed against
161 mCherry and pS269. Indeed, α-pS269 antibodies recognized $Su(H)^{gwt\text{-}mCh}$ protein specifically
162 in wasp infested larvae, indicating respective phosphorylation of Su(H) protein. No such signals
163 were seen in precipitates from the non-infected larvae nor from any of the $Su(H)^{S269A\text{-}mCh}$ mutant
164 larvae (Fig. 2B). These data clearly show that wasp infestation induced the phosphorylation of

165 Su(H) at S269. Apparently, parasitoid wasp infestation starts a cascade of events resulting in
166 the inhibitory S269 phosphorylation of Su(H) protein to promptly interrupt Notch signalling
167 activity and to allow lamellocyte formation. Hence, the question arose on the kinase/s involved
168 in this process.
169
170 ***Screening of kinase candidates mediating phosphorylation of Su(H) at Serine 269***
171 To identify Ser/Thr kinases involved in the phosphorylation of Su(H) at S269, we commenced
172 with a combination of *in silico* and biochemical approaches aiming to generate a list of
173 candidate kinases which can be further analysed by genetic means (Fig. 3). First, by using GPS
174 3.0 software that encompasses a substantial database of kinases and their preferred recognition
175 motives (Xue et al., 2011), 36 potential human kinases were predicted to recognize S269 as
176 substrate, represented by 30 kinases in *Drosophila* (Fig.3 – supplement Table 1). In addition,
177 the BTD domain of Su(H) was bacterially expressed as a GST fusion protein and subjected to
178 phospho-assays using 245 different human Ser/Thr kinases. Our reasoning for using the entire
179 BTD domain was to ensure a normal folding of the domain (Kovall and Blacklow, 2010), and
180 to reduce the number of potential phospho-sites at the same time present in full length Su(H).
181 With this approach, we ended up with 62 human Ser/Thr kinases (25% of the tested kinases)
182 that use the BTD of Su(H) as an *in vitro* substrate. These kinases correspond to 40 different
183 kinases in *Drosophila* belonging to six different kinase families (Fig.3 –supplement Table 2).
184 Ten of these kinases were also predicted *in silico*, representing members of the AGC, CAMK,
185 CMGC, STE and OPK family of kinases (Fig.3 –supplement Table 2). Both sets of data,
186 biochemical and bioinformatics, were used to generate a list of 44 candidates to be analysed by
187 genetic means (Fig.3 –supplement Table 3). The candidates were further screened for an
188 imbalanced hematopoiesis. We reasoned that mutants affecting a relevant kinase gene involved
189 in the phosphorylation of Su(H) should display increased crystal cell numbers similar to what
190 was observed in the $Su(H)^{S269A}$ mutant (Frankenreiter et al., 2021). Larvae of 13 different kinase
191 mutants and the progeny of 44 UAS-RNAi and/or UAS-kinase dead transgenes crossed with
192 *hml*-Gal4, a blood cell-specific Gal4 driver line, were tested (Fig.3 –supplement Table 3). To
193 this end, the larvae were subjected to heating. This procedure allows a comfortable visualization
194 and quantification of mature larval crystal cells through the cuticle, which blacken due to the
195 activation of Prophenoloxidase (Rizki, 1957; Lanot et al., 2001). Fourteen kinase mutants tested
196 were similar to the control, whereas mutations in four kinases impeded crystal cell development
197 or prevented it altogether. Unexpectedly, the majority of the tested kinase mutants exhibited
198 elevated crystal cell numbers, however to a different degree (Fig.3 –supplement Table 4). Seven

199 kinase mutants substantially exceeded crystal cell numbers seen in *Su(H)*^{S269A} larvae; they were
200 hence excluded from further analysis. Nineteen kinase mutants matched closely the *Su(H)*^{S269A}
201 phenotype, making those the most promising candidates for being involved in the
202 phosphorylation of Su(H) at S^{269}. Six of those were within the cluster of ten candidates singled
203 out by the *in silico* and the *in vitro* screens (Fig. 3 A,B). Using commercially available, activated
204 human kinases, we were able to test five candidates, AKT1, CAMK2D, GSK3B, S6 and
205 PKCα in vitro by MS/MS analysis on the Su(H) peptide ALFNRLR**S**^{8}QTVSTRY, where
206 Serine 8 corresponds to S269 in Su(H). Only PKCα unambiguously phosphorylated the given
207 peptide at Serine 8. Whereas GSK3B did not phosphorylate the peptide at all, AKT1, CAMK2D
208 and S6 piloted Threonine 10, corresponding to Threonine 271 in Su(H) (Fig. 3D- figure
209 supplement 1). Together, these data support the idea, that PKCα corresponding to Pkc53E in
210 *Drosophila*, is part of the kinase network mediating the phosphorylation of Su(H) at S269.
211
212 ***Role of Pkc53E in the phosphorylation of Su(H)***^{S269}
213 Confirming the MS/MS data, human PKCα was able to phosphorylate the respective Su(H)
214 peptide (S^{wt}) similar to its defined pseudo-substrate PS (Kochs et al., 1993), whereas the S8A
215 mutant peptide (S^{SA}) was accepted only half as well in an ADP-Glo™ assay, indicating that
216 S269 is a preferred substrate (Fig. 4A). Bacterially expressed and purified *Drosophila* Pkc53E,
217 however, did neither accept the PS nor the Su(H) peptides (Fig. 4B). Pkc53E activity, however,
218 was stimulated by the agonistic phorbol ester PMA (phorbol 12-myristate 13-acetate)
219 (Blumberg et al., 1983; Nakashima, 2002) in phosphorylating the PS and Su(H) peptide S^{wt} but
220 not the S8A mutant peptide S^{SA} (Fig. 4C). To generate an activated form of Pkc53E, we
221 exchanged four codons by *in vitro* mutagenesis, three (T508D, T650D and S669D) mimicking
222 phosphorylation in the kinase and C-terminal domains, respectively, and one in the pseudo-
223 substrate domain (A34E) (Fig.4 – figure supplement 1) (Gould and Newton, 2008). The
224 resultant Pkc53E^{EDDD} protein accepted the PS, and the Su(H) peptide S^{wt} even better, but not
225 the S8A mutant peptide S^{SA}, demonstrating the specificity of the phosphorylation (Fig. 4D). As
226 predicted for a fully activated kinase, PMA was unable to boost Pkc53E^{EDDD} protein activity
227 any further (Fig. 4E).
228
229 ***The PKC-agonist PMA influences Su(H) activity and blood cell homeostasis***
230 Our data so far indicated that Su(H) is a phospho-target of Pkc53E which reduces its activity
231 by affecting its DNA-binding. In this case, we might expect an influence of the general PKC-
232 activator PMA on both, Su(H) activity as well as Notch-mediated crystal cell formation. We

233 tested the former in a *RBPJ*^{ko} HeLa cell system (Wolf et al., 2019), measuring Notch-reporter
234 gene activation by Su(H)-VP16, as this Su(H) variant is independent of Notch activity itself,
235 allowing to directly monitor the influence of PMA on Su(H) activity. Indeed, Su(H)-VP16
236 ability to activate reporter gene transcription was reduced by more than half in the presence of
237 PMA (Fig. 5A). This is in agreement with an PMA-mediated activation of endogenous PKC in
238 the transfected HeLa cells, resulting in Su(H)-VP16 phosphorylation, loss of DNA-binding
239 activity and reduced transcriptional activation. Accordingly, repression could be reverted by
240 the addition of kinase-inhibitor Staurosporine (Karaman et al., 2008). In fact, Staurosporine
241 alone already increased Su(H)-VP16 transcriptional activity, indicating that PKC-driven
242 phosphorylation occurs to a considerable degree in the normal situation in HeLa cells already
243 (Fig. 5A).
244 Next, we assayed the effect of PMA on larval crystal cell formation. If, as expected, PMA
245 increased Pkc53E activity, Su(H) should be inactivated by phosphorylation with decreased
246 crystal cell numbers as a consequence. We fed PMA to *Drosophila* larvae and assayed the
247 numbers of sessile crystal cells. Indeed, crystal cell numbers dropped to nearly zero, similar of
248 what is observed in the phospho-mimetic *Su(H)*^{S269D} mutant (Frankenreiter et al., 2021),
249 suggesting a very efficient phosphorylation and inactivation of Su(H) protein (Fig. 5B). In
250 contrast, *Su(H)*^{S269A} mutant larvae displayed an increased number of crystal cells which can be
251 attributed to the fact that here, Su(H) can no longer be phosphorylated and hence, is overactive
252 in this context. Feeding PMA to *Su(H)*^{S269A} larvae only caused a drop of excessive crystal cell
253 numbers down to a wild type level (Fig. 5B). In conclusion these data show that Su(H) activity
254 is regulated *in vitro* and *in vivo* by PKC activity in the context of blood cell homeostasis.
255
256 ***Pkc53E is required for normal blood cell homeostasis in Drosophila larvae***
257 *Su(H)*^{S269A} mutant larvae develop an excess of crystal cells, both in the hemolymph as well as
258 in the lymph glands, due to a failure to downregulate respective Notch activity in the hemocyte
259 precursors via the phosphorylation of Su(H) protein (Frankenreiter et al., 2021) (see Fig. 1A).
260 Assuming Pkc53E has a major role in the phosphorylation of Su(H), we should expect a similar
261 phenotype in a *Pkc53E* mutant due to the inability to phosphorylate any substrate. In order to
262 test this assumption directly, we assessed the number of crystal cells in larval lymph glands as
263 well as in sessile crystal cells in several loss of function backgrounds of *Pkc53E*. To this end,
264 we used the *Pkc53E*$^{\Delta 28}$ allele, which by RT-PCR is a null mutation (Fig. 6 – figure supplement
265 1). In addition, we used two different RNAi-lines and one sgRNA line under UAS-control to
266 knock down *Pkc53E* activity specifically within the developing lymph gland using *lz*-Gal4 and

267 within the hemocytes using *hml*-Gal4, respectively (Lebestky et al., 2000). In any context
268 tested, the number of crystal cells was strongly increased matching those of the *Su(H)*^{S269A}
269 mutant (Fig. 6). The similar phenotypes imply that Pkc53E acts through the phosphorylation of
270 Su(H). However, as outlined above, the majority of kinase mutants displayed increased crystal
271 cell numbers, raising the possibility of a fortuitous accordance. If the increase of crystal cell
272 numbers in *Pkc53E* mutants is independent of Su(H) phosphorylation, we should expect an
273 additive effect if we combine the two mutants. The double mutants *Su(H)*^{S269A} *Pkc53E*$^{\Delta 28}$ were
274 generated by genetic recombination; they displayed the same range of excessive crystal cell
275 numbers as the single mutants (Fig. 7A,B). Moreover, the strongly reduced number of crystal
276 cells observed in the overactive *Su(H)*^{S269D} mutant was not increased by *Pkc53E*$^{\Delta 28}$ (Fig. 7A,B),
277 indicating that Pkc53E indeed acts upstream of Su(H), or directly on Su(H). If the latter is the
278 case, we may expect the two proteins to form complexes *in vivo*. Indeed, we could co-precipitate
279 Su(H)-Pkc53E protein complexes, both from *Drosophila* heads containing hemocytes (Sanchez
280 Bosch et al., 2019), as well as from the larval hemolymph (Fig. 7C,D). Specific co-precipitation
281 was eased by using fly strains expressing m-Cherry tagged Su(H) (Praxenthaler et al., 2017)
282 and HA-tagged Pkc53E, respectively. Together, these data demonstrate that *Pkc53E* has an
283 important role in blood cell homeostasis that can be largely explained by its activity to
284 phosphorylate Su(H), thereby regulating Notch activity during hemocyte and lymph gland
285 development.
286
287 ***Pkc53E mutants are immune compromised***
288 According to our hypothesis, Pkc53E phosphorylates Su(H) in response to an immune
289 challenge by parasitic wasp infestation. Hence, we would expect that a loss of Pkc53E function
290 should affect the ability of *Drosophila* larvae to fight wasp infestations similarly to the
291 *Su(H)*^{S269A} mutant. Indeed, when the *Pkc53E*$^{\Delta 28}$ null mutant was infested with the parasitic wasp
292 *L. boulardi*, lamellocyte numbers in the hemolymph did not reach wild type levels, and they
293 were absent from the larval lymph glands (Fig. 7E,F). Apparently, the *Pkc53E*$^{\Delta 28}$ null mutant
294 is unable to recognize parasitic wasp infestation or is unable to respond to it, for example by
295 the phosphorylation of Su(H), demonstrating the involvement of this kinase in the immune
296 response of *Drosophila* to parasitoid wasp infestation.

297

298 **Discussion**

299

300 The Notch pathway is highly conserved between invertebrates and vertebrates, with regard to
301 both the underlying molecular principles as well as the biological processes it is involved,
302 including hematopoiesis and immune defence. During mammalian hematopoiesis, Notch plays
303 a fundamental role in stem cell maintenance and proliferation as well as in the differentiation
304 of blood cell precursors, notably in T-cell development. Accordingly, aberrant Notch signaling
305 activity has profound consequences for blood cell homeostasis that may result in leukemia
306 (reviewed in: Radtke et al., 2010; Siebel and Lendahl, 2017; Banerjee et al., 2019; Gallenstein
307 et al., 2023). Hence, the principles of the regulation of Notch signaling activity are of great
308 interest.
309 Notch signals are transduced by CSL-type DNA-binding proteins that are pivotal to Notch
310 pathway activity, as no signal transduction could occur in their absence or in the instance of a
311 lack of DNA-binding. CSL proteins are extremely well conserved. They act as a molecular
312 switch, either activating or repressing Notch target genes, depending on the recruited cofactors.
313 Upon ligand binding, the Notch receptor is cleaved, and the biologically active Notch
314 intracellular domain (NICD) is released, to assemble an activation complex with CSL and
315 further co-factors. Notch pathway repression, however, entails for example the recruitment of
316 co-repressors by CSL; in *Drosophila* mediated by the binding of Hairless (reviewed in: Maier,
317 2006; Borggrefe and Oswald, 2009; Kovall and Blacklow, 2010; Bray, 2016; Giaimo et al.,
318 2021).
319 Studies of *Drosophila* hematopoiesis have uncovered a pleiotropic role of Notch in all the
320 hematopoietic compartments, where Notch activity needs to be precisely regulated to ensure
321 blood cell homeostasis (reviewed in: Banerjee et al., 2019; Csordás et al., 2021). During blood
322 cell formation, Notch directs the crystal cell lineage. Accordingly, a downregulation of Notch
323 activity causes a lack of crystal cells, whereas a gain of Notch activity results in increased
324 numbers (Duvic et al., 2002; Lebestky et al., 2003; Terriente-Felix et al., 2013; Gosh et al.,
325 2015; Frankenreiter et al., 2021). In our earlier work, we have shown that the regulation of
326 Notch activity during hemocyte differentiation is independent of the general Notch antagonist
327 Hairless. Instead, it relies on the post-translational modification of the *Drosophila* CSL protein
328 Su(H) (Frankenreiter et al., 2021). Phosphorylation at Ser269 in the beta-trefoil domain of
329 Su(H) impedes DNA-binding activity, and hence the capability of Su(H) to act as a
330 transcriptional regulator in the context of blood cell development, without affecting Su(H)

331 protein expression (Nagel et al., 2017; Frankenreiter et al., 2021). Accordingly, phospho-
332 deficient *Su(H)*^{S269A} mutants develop an excess of crystal cells. Now we provide evidence that
333 Su(H) phosphorylation is likewise involved in parasitoid wasp defense, pointing to a dual use
334 of the Notch pathway in blood cell homeostasis as well as in stress response, which is typical
335 for the myeloid system (Banerjee et al., 2019).
336 The primary cellular immune response of *Drosophila* to fight parasitoid wasp infestation is an
337 encapsulation of the parasite egg to terminate its further development. Albeit metabolically
338 extremely costly, *Drosophila* larvae have to remodel their entire hematopoietic system to
339 generate the masses of lamellocytes required for the encapsulation (reviewed in Letournau et
340 al., 2016; Kim-Jo et al., 2019; Csordás et al., 2021; Hultmark & Ando, 2022). There are two
341 major sources for the lamellocytes. One is the transdifferentiation of circulating plasmatocytes,
342 released from the sessile compartment and proliferating upon immune challenge (Márkus et al.,
343 2009; Honti et al., 2010; Stofanko et al., 2010; Vanha-Aho et al., 2015; Anderl et al., 2016).
344 Second is a massive expansion of prohemocytes in the lymph gland followed by a
345 differentiation to lamellocytes and their release due to the premature disintegration of the gland
346 (Lanot et al., 2001, Sorrentino et al., 2002, Louradour et al., 2017; Cho et al., 2020). Wasp
347 infestation hence provokes a biased commitment to the lamellocyte lineage at the expense of
348 crystal cells, as the two lineages are mutually exclusive (Krzemien et al., 2010; Tattikota et al.,
349 2020; Cho et al., 2020).
350 The processes underlying the *Drosophila* immune response to wasp parasitism are well-
351 understood, sharing many molecular details with the inflammatory responses of vertebrates
352 (reviewed in Letourneau et al., 2016; Kim-Jo et al., 2019; Banerjee et al., 2019; Kharrat et al.,
353 2022). Interestingly, sterile injury of *Drosophila* larvae initiates a likewise immune response
354 covering all aspects of wasp-mediated immune challenge (Evans et al., 2022). The epidermal
355 penetration by the wasp ovipositor causes a burst of hydrogen peroxide at the injury site via the
356 activation of the NADPH oxidase DUOX. The oxidative stress then induces a systemic
357 activation of Toll/NF-κB and JNK-signaling within circulating hemocytes as well as within the
358 cells of the posterior signaling center of the lymph gland. Following cytokine release,
359 JAK/STAT and EGFR signalling pathways are activated non-cell autonomously driving the
360 trans/differentiation of pro/hemocytes to lamellocyte fate and lymph gland dispersal (Nappi et
361 al., 1995; Schlenke et al., 2007; Sinenko et al., 2011; Gueguen et al., 2013; Razzell et al., 2013;
362 Louradour et al., 2017; Chakrabarti and Visweswariah, 2020; Evans et al., 2022; reviewed in
363 Letourneau et al., 2016; Banerjee et al., 2019). Whereas the switch to lamellocyte fate is well
364 elaborated, less is known about the processes underlying the simultaneous suppression of

365 crystal cell fate. Obviously, this step requires a downregulation of Notch signalling activity, as
366 the Notch pathway is instrumental to crystal cell fate in all the hematopoietic compartments
367 (Duvic et al., 2002; Lebestky et al., 2003; Schlenke et al., 2007; Small et al., 2014; reviewed in
368 Banerjee et al., 2019). Our work now reveals that a parasitoid wasp attack causes a
369 phosphorylation of Su(H) on Ser269 as means of an efficient, rapid and reversible way to inhibit
370 Notch activity. This idea is consistent with earlier observations, whereby wasp parasitism
371 quenched the expression of a Su(H)-lacZ reporter (Small et al., 2014). Moreover, we provide
372 evidence that Pkc53E is involved in Su(H) phosphorylation during blood cell development as
373 well as during parasitoid wasp-defense in *Drosophila*. The antagonistic role of Pkc53E in blood
374 cell homeostasis is fully consistent with earlier reports demonstrating that a loss of Pkc53E
375 activity increased the expansion of prohemocytes in a genetic model of myeloid leukemia in
376 *Drosophila* (Sinenko et al., 2010). Moreover, the involvement of PKCs in wasp defense is not
377 completely unexpected given their well-documented role in the immune responses of mammals
378 and *Drosophila* alike. For example, *Drosophila* flies ensure a healthy gut-microbiota
379 homeostasis by modulating DUOX activity as a pathogen-specific defense line (reviewed in
380 Kim and Lee, 2014). DUOX activation and ROS production, induced by gut pathogens was
381 shown to be mediated by Pkc53E and Ca^{2+} via phospholipase Cβ (Ha et al., 2009; Lee et al.,
382 2015). Sterile wounding of the *Drosophila* embryo triggers an instantaneous Ca^{2+} flash
383 followed by hydrogen peroxide production (Razzel et al., 2013). It is conceivable that the
384 epidermal breach by the wasp's sting similarly induces a Ca^{2+} flash that may spark Pkc53E
385 activation as a result. However, PKCs may be activated directly by oxidative modification even
386 in the absence of Ca^{2+}. Moreover, they may promote endogenous ROS production in a positive
387 feed back loop (reviewed in Cosentino-Gomes et al., 2012), that could support the systemic
388 response in the larval lymph gland.
389 The role of PKCs in the mammalian hematopoietic and immune systems is well documented.
390 PKCs in this context act redundantly, and presumably, this holds also for *Drosophila* where
391 several PKCs exist. Upon activation, PKCs may translocate into the nuclear compartment,
392 where they can directly influence gene expression programs, for example by piloting chromatin
393 factors as substrates, pivotal for regulating immune cell differentiation (reviewed in Lim et al.,
394 2015). PKCs, including PKCα, are present in CD34+ long-term hematopoetic stem cells.
395 Moreover, specific roles in both the myeloid and the multilymphoid lineages are known.
396 Notably, some PKC isoforms including PKCα may play a role in Notch-dependent T-cell
397 development. Notch pathway activity is indispensable for T-cell lineage commitment of early
398 thymic progenitors, however, is rapidly downregulated after the β-selection phase. As treatment

399 with phorbol ester upregulates the transcription of TCRα and β chains, a role of PKC in Notch-
400 dependent commitment of αβ T-cells has been proposed. With the expressing of the invariant
401 TCR components, fate commitment of T-cells driven by Notch signaling is completed.
402 Subsequent cell survival and differentiation into CD4+CD8+ double positive cells, however,
403 depends on the formation of a pre-TCR complex and requires PKCα activity (reviewed in
404 Altman and Kong, 2016; Yui and Rothenberg, 2014). During initial T-cell development,
405 Notch1 signaling increases in intensity in the pre-β-selected thymocytes due to an
406 autoregulatory feedback loop directly controlled by E proteins and by Notch1-CSL itself.
407 Following β-selection, as Notch signaling activity becomes dispensable, Notch1 is abruptly
408 downregulated at the transcriptional level. This rapid downregulation is mediated by the
409 inhibition of the E proteins (Yashiro-Ohtani et al., 2009), however, might in addition involve
410 the phosphorylation of CSL by PKCα. Cell fate in more mature thymocytes is then fixed by the
411 silencing of Notch target genes through chromatin modulators (reviewed in Yui and
412 Rothenberg, 2014).
413 Appropriate silencing of Notch signaling activity in the course of T-cell development is of
414 utmost importance, as prolonged Notch activity during β-selection predisposes the T-cells to
415 leukemic transformation. Phosphorylation of CSL proteins by PKCα kinase offers a way for a
416 rapid and reversible deactivation of Notch signals not only in *Drosophila* but also in the
417 mammalian system. In fact, the amino acid sequences harboring the respective Serine residue
418 in the CSL beta-trefoil domain are completely conserved between vertebrates and invertebrates
419 (Wilson and Kovall, 2006; Nagel et al., 2017), raising the possibility of a likewise regulatory
420 mechanism in mammalian hematopoiesis and immunity. Indeed, respective phosphorylation of
421 the human CSL protein at the homologous position Ser195 was observed in human embryonic
422 stem cells, where differentiation was induced by phorbol ester treatment (Rigbolt et al., 2011),
423 consistent with an involvement of PKCα in this context as well. In conclusion, our work
424 uncovers an important role for PKC-mediated downregulation of Notch activity via CSL-
425 phosphorylation in blood cell homeostasis and in the immune response to parasitoid wasp
426 infestation in *Drosophila*. Future work may uncover, whether the same mechanisms apply to
427 mammalian hematopoiesis and immunity as well.

428 **Materials and Methods**

429 **Key resources are listed in S1 Table**

430

431 ***Maintenance of parasitoid wasps and infection assay of Drosophila melanogaster***

432 *Leptopilina boulardi* (*L. boulardi*), *Leptopilina heterotoma* (*L. heterotoma*) and *Asobara*
433 *japonica* (*A. japonica*) were kindly provided by B. Häußling and J. Stöckl, Bayreuth, Germany
434 (Weiss et al., 2015). Wasp species were co-cultured with wild-type *Drosophila* larvae at room
435 temperature. To this end, about forty 3-5 days old female wasps and twenty male wasps were
436 co-incubated with second instar larvae for 5-7 days at room temperature. Every other day, fresh
437 drops of honey water were added to the vial plug for feeding the wasps. After two weeks, all
438 hatched flies were discarded. Wasps emerge about 30 days after the infestation.
439 For the infection assays, 50-100 staged *Drosophila* late second/early third instar larvae of the
440 respective genotype were transferred onto apple juice plates with fresh yeast paste. 30 females
441 and 20 males of the wasps aged between 3-6 days were added to the larvae, allowing to infect
442 them for 4-6 hours. Afterwards, wasps were removed and infected larvae were allowed to
443 develop further in vials with normal fly food. Wasps were only used once for each infection.
444 After infestation, third instar larvae were prepared, or the survival rate of wasps versus
445 *Drosophila* imago was recorded.

446

447 ***Fly work and genetic analyses***

448 Fly crosses were performed with 30-40 virgin females and 20 males to avoid overcrowding and
449 stress. Combination/recombination of fly stocks was monitored by PCR-genotyping using
450 primers listed in S2 Table. A complete list of the Kinase mutant flies tested in the 'larval kinase
451 screen' is found in Fig.3 – supplement Table 3. As reporter lines served *atilla*-GFP (BL23540)
452 and *PPO3*-Gal4 UAS mCD8-GFP (named *PPO3::GFP*, Dudzic et al., 2015). For Gal4/UAS
453 based overexpression and RNAi-mediated knockdown, we used *hml*-Gal4 (BL30141), *lz*-Gal4
454 (Lebestky *et al.*, 2000; obtained form M. Crozatier, Université de Toulouse, France), UAS-
455 *μMCas9* (VDRC 340002), UAS-HA-Pkc53E (this study), UAS-*white-RNAi* (BL31231) and
456 UAS-*sgRNA-Pkc53E* (VDRC341127). The strain *vasa-φC31*, *96E-attB*/TM3 (Bischof *et al.*,
457 2007) served for the generation of UAS-HA-Pkc53E flies. Su(H) controls and mutants
458 comprised: $Su(H)^{gwt}$, $Su(H)^{gwt\text{-}mCh}$, $Su(H)^{S269A}$ and $Su(H)^{S269D}$/*CyO-GFP*, (Praxenthaler *et al.*,
459 2017; Frankenreiter et al., 2021). $Su(H)^{S269A\text{-}mCh}$ flies were produced in this study by a C-
460 terminal in frame fusion of mCherry to the $Su(H)^{S269A}$ mutant gene followed by genomic
461 integration of the construct via gene engineering as outlined before (Praxenthaler *et al.*, 2017).

462

463 ***Generation of the UAS-HA-Pkc53E fly line***

464 *Pkc53E* cDNA (DGRC GH03188) was PCR amplified and subcloned via *Xho*I/*Xba*I in a
465 modified pBT-HA vector, harbouring three copies of an HA-Tag generated via annealed oligos
466 cloned into *Acc*65I/*Xho*I to generate pBT-3xHA-*Pkc53E*. HA-*Pkc53E* was then shuttled via
467 *Acc*65I/*Xba*I in likewise opened pUAST-attB vector (Bischof et al., 2007). All cloning steps
468 were sequence verified. Primers used for cloning are included in S2 Table. Transgenic fly lines
469 were then generated with the help of the PhiC31 integrase-based system using 96E as landing
470 site (Bischof et al., 2007).

471

472 ***RT-PCR of Pkc53E$^{\Delta 28}$ null mutants***

473 Poly(A)$^{+}$ RNA was isolated from 50 third instar larvae (*Pkc53E$^{\Delta 28}$* and *y^{1}w^{67c23}*) using
474 PolyATract System Kit 1000 (Promega, Mannheim, Germany) according to the manufacturer's
475 protocol, followed by a DNase I treatment (New England Biolabs GmbH, Frankfurt, Germany,
476 #M0303). Subsequent cDNA synthesis was conducted with qScriber cDNA Synthesis Kit
477 (highQu, Kraichtal, Germany) according to the supplier's protocol. For amplification, a *Pkc53E*
478 primer pair overlapping the last three introns was chosen (Pkc53E_RT-PCR UP and
479 Pkc53E_RT-PCR LP). Tubulin 56D primers (Tub56D_229 UP and Tub56D_507 LP) were
480 used as internal controls. For primers, see S2 Table.

481

482 **<u>Analyses of *Drosophila* hematopoetic cells and tissues</u>**

483 ***Determination of sessile larval crystal cells***

484 Larval crystal cells were counted according to Frankenreiter *et al.*, 2021. Briefly, staged
485 wandering third instar larvae of the respective genotype were heated to 60°C for 10-12 min.
486 Pictures of the posterior dorsal side were taken with a Pixera camera (ES120, Optronics, Goleta,
487 USA) mounted to a stereo-microscope (Wild M3Z, Leica, Wetzlar, Germany) with Pixera
488 Viewfinder 2.5. Melanized crystal cells appear as black dots, and were counted in the last two
489 larval segments with *ImageJ* 1.51 software using *Cell Counter* tool. 25-74 larvae were scored
490 for the statistical evaluation. For the PMA-feeding experiment, 20-30 developmentally
491 synchronized second instar larvae were selected and grown for 24 h in complete dark at 25ºC
492 on fly food with 500 µl of 1 mM Phorbol-12-myristat-13-acetat (PMA, Sigma-Aldrich, St.
493 Louis, USA) added to the surface. Subsequently, wandering third instar larvae were heated and
494 analysed as above.

495 ***Visualization and quantification of lamellocytes***

496 The lamellocyte specific reporters *atilla*-GFP or *PPO3*::GFP strains were re/combined with
497 *Su(H)*^{gwt}, *Su(H)*^{S269A} or *Pkc53E*$^{\Delta 28}$ alleles by genetic means. Late second/early third larval
498 instars were infested by *L. boulardi* and the number of lamellocytes was determined two days
499 later and compared with those observed in non-infested larvae. Larvae were washed thoroughly
500 in cold PBS and dried with a tissue and teared apart. The hemolymph of 10 larvae each was
501 collected with a 20 µl Microloader tip (Eppendorf, Hamburg, Germany) and placed on a slide
502 with 7 µl of Vectashield mounting medium containing DAPI (BIOZOL, Eching, Germany).
503 GFP-positive cells, i.e. lamellocytes were counted in relation to the total number of DAPI
504 labelled hemocytes with a Zeiss Axioskop and a PlanNeofluar 20x objective. 8-10 independent
505 bleedings were performed each.

506 ***Immunostaining and documentation of larval lymph glands***

507 Larval lymph glands were prepared one-two days after infection and treated as described before
508 (Frankenreiter *et al.*, 2021). For comparison, non-infested lymph glands were prepared.
509 Primary antibodies used for staining: mouse anti-Hnt for crystal cells (DSHB 1G9, RRID:
510 AB_528278, 1:20) and guinea pig anti-Pzg as nuclear marker (Kugler and Nagel, 2007; 1:500).
511 GFP signals were monitored directly. Secondary fluorescent antibodies were from Jackson
512 Immuno-Research Laboratories (obtained from Dianova, Hamburg Germany, 1:250 each).
513 Mounted tissue was documented with a Zeiss Axioskop coupled with a BioRad MRC1024
514 confocal microscope using LaserSharp software 2000. For statistical evaluation at least 12
515 primary lobes were documented and statistically analyzed by using *Image J* software
516 (Schindelin et al., 2012). Indices represent the number of cells in relation to the size/area of the
517 tissue (in pixel) x 10000.

518

519 **<u>Determination of kinases and kinase assays</u>**

520 ***Screening of protein kinase candidates in silico and in vitro***

521 To search for potential candidates in silico, GPS3.0 software was used at the lowest threshold
522 levels, including the 40 kinases with the highest difference between score and cut-off value
523 (Xue *et al.*, 2011). The corresponding *Drosophila* kinases were determined with the help of
524 flybase according to (Morrison et al., 2000). For the *in vitro* screen, a 0.5kb cDNA fragment
525 (741-1242) encoding the Su(H) beta-trefoil domain (codons 247-414), was PCR-amplified and
526 cloned via *Bam*HI/ *Eco*RI into pGEX-2T vector (Smith and Johnson, 1988) for bacterial
527 expression and purification of the BTD-GST fusion protein. Primers used for cloning are
528 included in S2 Table. ProQinase GmbH (Freiburg, Germany) provided the 'KinaseFinder assay
529 service'. Briefly, BTD-GST and ^{33}P-ATP served as substrates for 245 human Ser/Thr kinases

530 in multi-well plates, analysed in a microplate scintillation reader. (A) Activity of each kinase
531 was determined, (B) corrected for substrate background activity, and (C) auto-phosphorylation
532 (kinase activity without substrate). A ratio value between phosphorylation of BTD-Su(H) and
533 kinase auto-phosphorylation >1 (A-B/C) was considered as significant.

534 ***In vitro ADP-Glo™ kinase assay***

535 *Drosophila* pBT-3xHA-*Pkc53E* was mutated to generate the pseudo-activated form
536 *Pkc53E*^{EDDD} (A34E/T508D/T650D/S669D) stepwise by site directed mutagenesis using the
537 Q5® Site directed Mutagenesis Kit (New England Biolabs, Frankfurt, Germany). Primers used
538 for mutagenesis are included in S2 Table. *Pkc53E* as well as *PKC53E*^{EDDD} were then shuttled
539 into a modified pMAL vector (Riggs, 1994) where additional restriction sites for *Acc*65I, *Sac*II
540 and *Xho*I had been included in the multiple cloning site via primer annealing. The MBP-Pkc53E
541 and MBP-Pkc53E^{EDDD} fusion proteins were bacterially expressed and purified with Amylose
542 resin (New England Biolabs, Frankfurt, Germany). Additionally, activated human kinase
543 PKCα was obtained for a positive control (ProQinase, Freiburg, Germany). The PKCα pseudo-
544 substrate PS (RFARLG**S**LRQKNV) (Kochs et al., 1993), the wild type Su(H) peptide S^{wt}
545 (ALFNRLR**S**QTVSTRY) and the phospho-deficient peptide S^{SA} (ALFNRLR**A**QTVSTRY)
546 were obtained (peptides & elephants, Henningsdorf, Germany).

547 To test kinase activity, the ADP-Glo™ Kinase Assay system (Promega, Madison, USA) was
548 used. Kinase assay reactions were performed in 96 well plates in a volume of 25 µl in the dark.
549 Each reaction contained 100 µM of a kinase substrate peptide, 150 ng purified kinase and 500
550 µM ultra-pure ATP. 150 nM Phorbol 12-myristate 13-acetate (PMA) (Sigma-Aldrich, St.
551 Louis, USA) was added to some reactions. The mixture was filled up with Kinase reaction
552 buffer (40 mM Tris-HCl, 20 mM $MgCl_2$, 0.1 mg/ml BSA, pH 7.4) and incubated at room
553 temperature for 1 h in the dark. 25 µl ADP-Glo Reagent were added and incubated for 40 min
554 to remove residual ATP. 50 µl of Kinase Detection Reagent was applied to convert ADP to
555 ATP. The luminescent signal was measured after 45 min using GloMax® Discover Microplate
556 Reader (Promega, Madison, USA), kindly provided by the Department of Zoology (190z),
557 University of Hohenheim.

558 ***NanoLC-ESI-MS/MS analysis of Su(H) peptides***

559 Nano-LC-ESI-MS/MS experiments were performed by the Mass Spectrometry Unit at the Core
560 Facility Hohenheim (640) on an Ultimate 2000 RSLCnano system coupled to a Nanospray Flex
561 Ion Source and a Q-Exactive HF-X mass spectrometer (Thermo Fisher Scientific, Waltham,
562 USA). Peptides were separated with LTQ-Orbitrap XL coupled to a nano-HPLC operated under
563 the control of XCalibur 4.1.31.9 software (Thermo Fisher Scientific, Waltham, USA). For all

564 measurements using the Orbitrap detector, internal calibration was as described before (Olsen
565 et al., 2005). MS/MS spectra were analyzed using Proteome Discoverer 2.2 (ThermoFisher
566 Scientific, Waltham, United States), verified by manual inspection of the MS/MS spectra
567 (Voolstra et al., 2010).
568
569 ***Generation of an α-pS269 antiserum***
570 Rabbit polyclonal p-S269 Su(H) antiserum was generated by DAVIDS Biotechnology GmbH
571 (Regensburg, Germany) using the synthetic phospho-peptide NLRL**pS**QTVSTRYLHVE.
572 Phospho-specific antibodies were enriched in a depletion-step by affinity purification against
573 the non-phosphorylated peptide.
574
575 ***Immunoprecipitation of mCherry and Myc-tagged Su(H)***
576 400 adult heads or 25 larvae of each genotype were homogenized on ice in 220 µl buffer 1 [150
577 mM NaCl, 1% Triton X-100, 50 mM Tris-HCl pH 7.5, 0.1% SDS, supplemented with protease
578 inhibitor cocktail (Roche, Basel, Switzerland)] and incubated for 15 min. After a short spin, 20
579 µl of the supernatant was set aside as input fraction ('protein extract'). The residual supernatant
580 was diluted with 300 µl wash buffer I (see buffer I without Triton X-100). 15 µl of equilibrated
581 magnetic RFP-Trap Agarose beads (ChromoTek, Planegg, Germany) were added, incubated
582 for 1 h at 8°C and washed three times with wash buffer I. mCherry-trapped proteins were
583 resolved on SDS-PAGE; Western blots were probed with rabbit anti-mCherry (GeneTex,
584 Irvine, USA, 1:1000, #GTX128508) and rat anti-HA (Roche, Basel, Switzerland, 1:500,
585 #11867423001). Goat secondary antibodies coupled with alkaline phosphatase (Jackson
586 Immuno Research Laboratories, 1:1000) were used for detection.
587
588 **<u>HeLa cell culture experiments and Luciferase assays</u>**
589 ***Generation of HSV-TK 2xMyc-Su(H)-VP16***
590 Two myc-tags were added to *Su(H)* cDNA in pBT (Maier et al., 2011) by insertion of the two
591 annealed oligonucleotides Myc-Tag UP and Myc-tag LP into the *Eco*RI site (for primers, see
592 S2 Table). The construct was subsequently shuttled via *Eco*RI/*Xho*I into pCDNA3.1
593 (Invitrogen, Thermo Fisher Scientific, Waltham, USA). A VP16 activator domain was then
594 cloned in frame at the C-terminus of 2xMyc-*Su(H)* by replacing the 829 bp *BspE*I/*Apa*I
595 fragment of pCDNA3 *2xMyc-Su(H)* with a respective1060 bp fragment of the pUAST *Su(H)-*
596 *VP16* construct (Cooper et al., 2000). Then the CMV Promotor of pCDNA3 2xMyc-Su(H)-
597 VP16 was replaced by the HSV-TK Promotor of the pRL TK Vector (Promega, Madison,

598 USA). To this end, the 1023 bp *Bgl*II/*Nhe*I fragment from pRL TK was cloned into the
599 *Bgl*II/*Spe*I opened pCDNA3 *2xMyc- Su(H)*^{VP16} construct.

600 ***Transfection of HeLa cells and reporter assay***

601 *RBPj*^{KO} HeLa cells were cultivated and transfected as described (Wolf et al., 2019). The
602 following constructs were used: pGL3 NRE-reporter (Bray et al., 2005), pCDNA3 HSV-TK
603 2xMyc Su(H)^{VP16} and pRL TK (Promega, Madison, USA). For the Luciferase assay, 1 x 10^5
604 HeLa *RBPj*^{KO} cells were seeded in each well of a 12-well cell culture plate. After 24 h the cells
605 were transfected with 500 ng pGL3 NRE-reporter, 460 ng pCDNA3 HSV-TK 2xMyc Su(H)^{VP16}
606 and 40 ng pRL-TK. 4 h after the transfection the cells were treated with 162 nM PMA (Sigma-
607 Aldrich, St. Louis, USA), 162 nM PMA plus 21,4 nM stauporine (STAU, Sigma-Aldrich, St.
608 Louis, USA) or 21,4 nM STAU alone. Control cells were treated with the same volume of
609 DMSO present in the other treatments. 14 hours later, cells were washed twice in PBS pH 7.4
610 and lysed in 75 µl 1x Passive Lysis Buffer (Promega, Madison, USA). The Dual-Luciferase®
611 Reporter Assay (Promega, Madison, USA) was performed according to the manufacturer's
612 instructions.

613

614 ***Statistical analysis and documentation of data***

615 Statistical significance of collected data was determined by a two-tailed analysis of variance
616 (ANOVA) approach for multiple comparisons according to Dunnett's Test and Tukey-
617 Kramer's Honestly Significance Difference with p-values ***, $p \leq 0.001$; **, $p \leq 0.01$; *, $p \leq 0.05$;
618 not significant, $p > 0.5$. Boxplots were created with BoxPlotR software (Spitzer et al. 2014).
619 Pictures were assembled using ImageJ, PhotoPaint, CorelDraw and BoxPlotR software.

620 **Data availability**

621 All data are contained within the manuscript.

622

623 **Acknowledgments**

624 We are deeply grateful to Benedikt Häußling and Johannes Stöckl (University of Bayreuth,
625 Germany) for sending us all wasp species used in this study and for giving LF and SD a basic
626 course in the handling of wasps. We thank Michèle Crozatier (Toulouse, France), David
627 Hipfner (Montréal, Canada), Bruno Lemaitre (Lausanne, Switzerland), Sarah Bray
628 (Cambridge, UK), Dieter Maier (Hohenheim, Germany), the Bloomington *Drosophila* Stock
629 Center (BDSC, NIH P40OD018537) and the Vienna *Drosophila* Stock Center (VDRC) for
630 numerous fly stocks. We acknowledge the Drosophila Genomics Resource Center (DGRC,
631 NIH 2P40OD010949) for sending the Pkc53E cDNA, and the Developmental Studies
632 Hybridoma Bank (DSHB), created by the NICHD of the NIH and maintained at the
633 University of Iowa, Department of Biology, Iowa City, IA 52242 for providing the Hnt (1G9)
634 antibody, developed by HD Lipshitz. We very much acknowledge Franz Oswald (Ulm,
635 Germany) and Tilman Borggrefe (Gießen, Germany) for the $RBPj^{KO}$ HeLa cell line. We are
636 indebted to Lisa Lermer for her help in tissue preparations and screening of larvae and Janika
637 Scharpf for the purification of the Pkc53E proteins. We are grateful to Armin Huber,
638 Department of Biochemistry, for the use of the Apotome microscope, to Axel Schweickert,
639 Department of Zoology, for use of the GloMax® Discover Microplate Reader and to Jens
640 Pfannstiel at the Mass Spectrometry Unit (Core Facility of the University of Hohenheim) for
641 the MS/MS and ESI spectra. We thank Dieter Maier for helpful comments on the manuscript.

642 **References**

643 Altman, A., Kong, K.F. (2016). Protein Kinase C Enzymes in the Hematopoietic and Immune
644 Systems. *Annu Rev Immunol*. 34:511-538. doi:10.1146/annurev-immunol-041015-055347
645 Anderl, I., Vesala, L., Ihalainen, T. O., Vanha-Aho, L. M., Andó, I., Rämet, M., Hultmark, D.
646 (2016). Transdifferentiation and Proliferation in Two Distinct Hemocyte Lineages in
647 *Drosophila melanogaster* Larvae after Wasp Infection. *PLoS Pathog*. 12(7):e1005746.
648 doi:10.1371/journal.ppat.1005746
649 Banerjee, U., Girard, J.R., Goins, L.M., Spratford, C.M. (2019). *Drosophila* as a genetic
650 model for hematopoiesis. *Genetics* 211(2):367-417. DOI: 10.1534/genetics.118.300223.
651 Bischof, J., Maeda, R.K., Hediger, M., Karch, F., Basler, K. (2007). An optimized
652 transgenesis system for *Drosophila* using germ-line-specific phiC31 integrases. Proc Natl
653 Acad Sci USA 104(9):3312-3317. doi:10.1073/pnas.0611511104
654 Blumberg, P.M., Delclos, K.B., Dunn, J.A., Jaken, S., Leach, K.L., Yeh, E. (1983). Phorbol
655 ester receptors and the in vitro effects of tumor promoters. *Ann N Y Acad Sci*. 407:303-315.
656 doi:10.1111/j.1749-6632.1983.tb47836.x
657 Borggrefe, T., Oswald, F. (2009). The Notch signaling pathway: transcriptional regulation at
658 Notch target genes. *Cell Mol Life Sci*. 66(10):1631-1646. doi:10.1007/s00018-009-8668-7
659 Bray, S.J. (2016). Notch signalling in context. *Nat Rev Mol Cell Biol*. 17(11):722-735.
660 doi:10.1038/nrm.2016.94
661 Bray, S., Musisi, H., Bienz, M. (2005). Bre1 is required for Notch signaling and histone
662 modification. *Dev Cell* 8(2):279-286. doi: 10.1016/j.devcel.2004.11.020
663 Chakrabarti, S., Visweswariah, S.S. (2020). Intramacrophage ROS Primes the Innate Immune
664 System via JAK/STAT and Toll Activation. *Cell Rep*. 33(6):108368.
665 doi:10.1016/j.celrep.2020.108368
666 Cherbas, L., Willingham, A., Zhang, D., Yang, L., Zou, Y., Eads, B.D., Carlson, J.W.,
667 Landolin, J.M., Kapranov, P., Dumais, J., *et al*. (2011). The transcriptional diversity of 25
668 *Drosophila* cell lines. *Genome Res*. 21(2):301-314. doi:10.1101/gr.112961.110
669 Cho, B., Yoon, S. H., Lee, D., Koranteng, F., Tattikota, S. G., Cha, N., Shin, M., Do, H., Hu,
670 Y., Oh, S. Y., *et al.* (2020). Single-cell transcriptome maps of myeloid blood cell lineages
671 in *Drosophila*. *Nat. Commun*. 11, 4483. doi:10.1038/s41467-020-18135-y.
672 Cosentino-Gomes, D., Rocco-Machado, N., Meyer-Fernandes, J. R. (2012). Cell signaling
673 through protein kinase C oxidation and activation. *Int J Mol Sci*. 13(9):10697-10721.
674 doi:10.3390/ijms130910697

675 Cooper, M.T., Tyler, D.M., Furriols, M., Chalkiadaki, A., Delidakis, C., Bray, S. (2000).
676 Spatially restricted factors cooperate with notch in the regulation of Enhancer of split
677 genes. *Dev Biol.*, *221*(2), 390–403. doi:10.1006/dbio.2000.9691
678 Crozatier, M., Ubeda, J.-M., Vincent, A., Meister, M., (2004). Cellular immune response to
679 parasitization in *Drosophila* requires the EBF orthologue collier. *PLoS Biol*. 2, E196.
680 doi:10.1371/journal.pbio.0020196
681 Csordás, G., Gábor, E., Honti, V. (2021). There and back again: The mechanisms of
682 differentiation and transdifferentiation in *Drosophila* blood cells. *Dev Biol*. 2021;469:135-
683 143. doi:10.1016/j.ydbio.2020.10.006
684 Dudzic, J.P., Kondo, S., Ueda, R., Bergman, C.M., Lemaitre, B. (2015). *Drosophila* innate
685 immunity: regional and functional specialization of prophenoloxidases. *BMC Biol* 13:81.
686 doi: 10.1186/s12915-015-01393-6
687 Duvic, B., Hoffmann, J.A., Meister, M., Royet, J. (2002). Notch signaling controls lineage
688 specification during *Drosophila* larval hematopoiesis. *Curr. Biol*. 12: 1923–1927.
689 doi:10.1016/s0960-9822(02)01297-6
690 Evans, C.J., Liu, T., Girard, J.R., Banerjee, U. (2022). Injury-induced inflammatory signaling
691 and hematopoiesis in *Drosophila*. *Proc Natl Acad Sci U S A*. 119(12):e2119109119.
692 doi:10.1073/pnas.2119109119
693 Ferguson, G.B., Martinez-Agosto, J. A. (2014) Yorkie and Scalloped signaling regulates
694 Notch-dependent lineage specification during *Drosophila* hematopoiesis. *Curr. Biol*. 24:
695 2665–2672. doi:10.1016/j.cub.2014.09.081
696 Frankenreiter, L., Gahr, B.M., Schmid, H., Zimmermann, M., Deichsel, S., Hoffmeister, P.,
697 Turkiewicz, A., Borggrefe, T., Oswald, F., Nagel, A.C. (2021). Phospho-site mutations in
698 transcription factor Suppressor of Hairless impact Notch signaling activity during
699 hematopoiesis in *Drosophila*. *Front Cell Dev Biol*. 9:658820. doi:
700 10.3389/fcell.2021.658820
701 Gallenstein, N., Tichy, L., Weigand, M.A., Schenz, J. (2023). Notch Signaling in Acute
702 Inflammation and Sepsis. *Int J Mol Sci*. 24(4):3458. doi:10.3390/ijms24043458
703 Giaimo B.D., Gagliani E.K., Kovall R.A., Borggrefe T. (2021). Transcription Factor RBPJ as
704 a Molecular Switch in Regulating the Notch Response. *Adv Exp Med Biol*. 1287:9-30.
705 doi:10.1007/978-3-030-55031-8_2
706 Ghosh, S., Singh, A., Mandal, S., Mandal, L. (2015). Active hematopoietic hubs in
707 *Drosophila* adults generate hemocytes and contribute to immune response. *Dev. Cell*
708 33:478-488. doi: org/10.1016/j.devcel.2015.03.014

709 Gould C.M., Newton A.C. (2008). The life and death of protein kinase C. *Curr Drug Targets*
710 9(8):614-625. doi:10.2174/138945008785132411
711 Gueguen, G., Kalamarz, M. E., Ramroop, J., Uribe, J., Govind, S. (2013). Polydnaviral
712 ankyrin proteins aid parasitic wasp survival by coordinate and selective inhibition of
713 hematopoietic and immune NF-kappa B signaling in insect hosts. *PLoS Pathog*.
714 9(8):e1003580. doi:10.1371/journal.ppat.1003580
715 Ha, E.M., Lee, K.A., Park, S.H., Kim, S.H., Nam, H.J., Lee, H.Y., Kang, D., Lee, W.J.
716 (2009). Regulation of DUOX by the Galphaq-phospholipase Cbeta-Ca2+ pathway in
717 *Drosophila* gut immunity. *Dev Cell*. 16(3):386-397. doi:10.1016/j.devcel.2008.12.015
718 Honti, V., Kurucz, E., Csordás, G., Laurinyecz, B., Márkus, R., Andó, I. (2009). In vivo
719 detection of lamellocytes in *Drosophila melanogaster*. *Immunol Lett.* 126(1-2):83-84. doi:
720 10.1016/j.imlet.2009.08.004
721 Honti, V., Csordás, G., Márkus, R., Kurucz, E., Jankovics, F., Andó, I. (2010). Cell lineage
722 tracing reveals the plasticity of the hemocyte lineages and of the hematopoietic
723 compartments in *Drosophila melanogaster*. *Mol Immunol*. 47(11-12):1997-2004.
724 doi:10.1016/j.molimm.2010.04.017
725 Hultmark, D., Andó, I. (2022) Hematopoietic plasticity mapped in *Drosophila* and other
726 insects. *Elife* 11:e78906. doi:10.7554/eLife.78906
727 Karaman, M.W., Herrgard, S., Treiber, D.K., Gallant, P., Atteridge C.E., Campbell, B.T.,
728 Chan, K.W., Ciceri, P., Davis, M.I., Edeen, P.T., *et al.* (2008). A quantitative analysis of
729 kinase inhibitor selectivity. *Nature Biotechnology* 26:127-132. doi: 10.1038/nbt1358.
730 Kharrat, B., Csordás, G., Honti, V. (2022). Peeling Back the Layers of Lymph Gland
731 Structure and Regulation. *Int J Mol Sci*. 23(14):7767. doi:10.3390/ijms23147767
732 Kim, S.H., Lee, W.J. (2014). Role of DUOX in gut inflammation: lessons from *Drosophila*
733 model of gut-microbiota interactions. *Front Cell Infect Microbiol*. 3:116.
734 doi:10.3389/fcimb.2013.00116
735 Kim-Jo C, Gatti J.L., Poirié M. (2019) *Drosophila* Cellular Immunity Against Parasitoid
736 Wasps: A Complex and Time-Dependent Process. *Front Physiol*. 2019;10:603.
737 doi:10.3389/fphys.2019.00603
738 Kochs, G., Hummel, R., Meyer, D., Hug, H., Marmé, D., Sarre, T.F. (1993). Activation and
739 substrate specificity of the human protein kinase C alpha and zeta isoenzymes. *Eur J*
740 *Biochem*. 216(2):597-606. doi:10.1111/j.1432-1033.1993.tb18179.x
741 Kopan R, Ilagan M.X. (2009). The canonical Notch signaling pathway: unfolding the
742 activation mechanism. *Cell* 137(2):216-233. doi:10.1016/j.cell.2009.03.045

743 Kovall, R.A., Blacklow, S.C. (2010). Mechanistic insights into Notch receptor signaling from
744 structural and biochemical studies. *Curr Top Dev Biol*. 92:31-71. doi:10.1016/S0070-
745 2153(10)92002-4
746 Krzemien, J., Oyallon, J., Crozatier, M., Vincent, A. (2010). Hematopoietic progenitors and
747 hemocyte lineages in the *Drosophila* lymph gland. *Dev. Biol*. 346, 310–319.
748 doi:10.1016/j.ydbio.2010.08.003
749 Kugler, S.J., Nagel, A.C. (2007). *Putzig* is required for cell proliferation and regulates Notch
750 activity in *Drosophila*. *Mol Biol Cell* 18(10):3733-3740. doi: 10.1091/mbc.e07-03-0263
751 Lanot, R., Zachary, D., Holder, F., Meister, M. (2001). Postembryonic hematopoiesis in
752 *Drosophila*. *Dev Biol*. 230, 243–257. doi: 10.1006/dbio.2000.0123
753 Lebestky, T., Chang, T., Hartenstein, V., Banerjee, U. (2000). Specification of *Drosophila*
754 hematopoietic lineage by conserved transcription factors. *Science* 288(5463):146-149.
755 doi:10.1126/science.288.5463.146
756 Lebestky, T., Jung, S.-H., Banerjee, U. (2003). A Serrate-expressing signaling center controls
757 *Drosophila* hematopoiesis. *Genes Dev* 17(3):348-353. doi: 10.11101/gad.1052803
758 Lee, K.A., Kim, B., Bhin, J., Kim, D.H., You, H., Kim, E. K., Kim, S.H., Ryu, J.H., Hwang,
759 D., Lee, W.J. (2015). Bacterial uracil modulates *Drosophila* DUOX-dependent gut
760 immunity via Hedgehog-induced signaling endosomes. *Cell Host Microbe* 17(2):191-204.
761 doi:10.1016/j.chom.2014.12.012
762 Letourneau, M., Lapraz, F., Sharma, A., Vanzo, N., Waltzer, L., Crozatier, M. (2016).
763 *Drosophila* hematopoiesis under normal conditions and in response to immune stress.
764 *FEBS Lett*. 590(22):4034-4051. doi: 10.1002/1873-3468.12327
765 Lim, P.S., Sutton, C.R., Rao, S. (2015). Protein kinase C in the immune system: from
766 signalling to chromatin regulation. *Immunology*. 146(4):508-522. doi:10.1111/imm.12510
767 Louradour, I., Sharma, A., Morin-Poulard, I., Letourneau, M., Vincent, A., Crozatier, M.,
768 Vanzo, N. (2017). Reactive oxygen species-dependent Toll/NF-KB activation in the
769 *Drosophila* hematopoietic niche confers resistance to wasp parasitism. *Elife* 6:e25496.doi:
770 10.7554/eLife.25496.
771 Maier, D. (2006). Hairless: the ignored antagonist of the Notch signalling pathway. *Hereditas*
772 143:212-221. doi: 10.1111/j.2007.0018-0661.01971.x
773 Maier, D., Kurth, P., Schulz, A., Russell, A., Yuan, Z., Gruber, K., Kovall, R.A., Preiss, A.
774 (2011). Structural and functional analysis of the repressor complex in the Notch signaling
775 pathway of *Drosophila melanogaster*. *Mol Biol Cell*. *22*(17), 3242–3252.
776 doi:10.1091/mbc.E11-05-0420.

Maier, D., Nagel, A.C., Kelp, A., Preiss, A. (2019). Protein kinase D is dispensable for development and survival of Drosophila melanogaster. G3(Bethesda) 9(8):2477-2487. doi:10.1534/g3.119.400307.

Márkus, R., Laurinyecz, B., Kurucz, E., Honti, V., Bajusz, I., Sipos, B., Somogyi, K., Kronhamn, J., Hultmark, D., Andó, I. (2009). Sessile hemocytes as a hematopoietic compartment in *Drosophila melanogaster*. *Proc Natl Acad Sci U S A*. 106(12):4805-4809. doi:10.1073/pnas.0801766106

Morrison, D.K., Murakami, M.S., Cleghon, V. (2000). Protein kinases and phosphatases in the *Drosophila* genome. *J Cell Biol* 150(2):F57-62. Doi: 10.1083/jcb.150.2.f57.

Nagel, A.C., Auer, J.S., Schulz, A., Pfannstiel, J., Yuan, Z., Collins, C. E., Kovall, R.A., Preiss, A. (2017). Phosphorylation of Suppressor of Hairless impedes its DNA-binding activity. *Sci Rep*. 7(1):11820. doi:10.1038/s41598-017-11952-0

Nakashima, S. (2002). Protein kinase C alpha (PKC alpha): regulation and biological function. *J Biochem*. 132(5):669-675. doi:10.1093/oxfordjournals.jbchem.a003272

Nappi, A.J., E. Vass, F. Frey, Y. Carton (1995). Superoxide anion generation in *Drosophila* during melanotic encapsulation of parasites. *Eur. J. Cell Biol*. 68: 450–456.

Olsen, J.V., de Godoy, L.M.F., Li, G., Mortensen, P., Pesch, R., Makarov, A., Lange, O., Horning, S., Mann, M. (2005). Parts per million mass accuracy on an Orbitrap mass spectrometer via lock mass injection into a C-trap. *Mol Cell Proteomics* 4(12):2010-2021. doi: 10.1974/mcp.T500030-MCP200

Praxenthaler, H., Nagel, A.C., Schulz, A., Zimmermann, M., Meier, M., Schmid, H., Preiss, A., Maier, D. (2017). Hairless-binding deficient Suppressor of Hairless alleles reveal Su(H) protein levels are dependent on complex formation with Hairless. *PLoS Genet*. 13(5):e1006774. doi: 10.1371/journal.pgen.1006774

Radtke, F., Fasnacht, N., Macdonald, H.R. (2010). Notch signaling in the immune system. *Immunity* 32(1):14-27. doi:10.1016/j.immuni.2010.01.004

Razzell, W., Evans, I.R., Martin, P., Wood, W. (2013). Calcium flashes orchestrate the wound inflammatory response through DUOX activation and hydrogen peroxide release. *Curr Biol*. 23(5):424-429. doi:10.1016/j.cub.2013.01.058

Rigbolt, K.T., Prokhorova, T.A., Akimov, V., Henningsen, J., Johansen, P.T., Kratchmarova, I., Kassem, M., Mann, M., Olsen, J.V., Blagoev, B. (2011). System-wide temporal characterization of the proteome and phosphoproteome of human embryonic stem cell differentiation. *Sci Signal*. 4(164):rs3. doi:10.1126/scisignal.2001570

Riggs, P. (1994) Expression and Purification of Maltose-Binding Protein Fusions. *Curr. Protoc. Mol. Biol. 28*, 16.6.1-16.6.14. 855 doi:10.1002/0471142727.mb1606s28. 856

Rizki, T.M. (1957). Alterations in the haemocyte population of *Drosophila melanogaster*. *J. Morphol*. 100, 437–458. doi: 10.1002/jmor.1051000303

Sanchez Bosch, P.S., Makhijani, K., Herboso, L., Gold, K.S., Baginsky, R., Woodcock, K.J., Alexander, B., Kukar, K., Corcoran, S., Jacobs, T., *et al.* (2019). Blood cell reservoir at the respiratory epithelia top relay infection signals to surrounding tissues. *Dev Cell* 51:787-803. doi: 10.1016/j.devcel.2019.10.017

Schindelin, J., Arganda-Carreras, I., Frise, E., Kaynig V, Longair M, Pietzsch T, Preibisch, S., Rueden, C., Saalfeld, S., Schmid, B., *et al.* Fiji: an open-source platform for biological-image analysis. *Nat Methods* 9, 676–682 (2012). doi:10.1038/nmeth.2019

Schlenke, T.A., Morales, J., Govind, S., Clark, A.G. (2007). Contrasting infection strategies in generalist and specialist wasp parasitoids of *Drosophila melanogaster*. *PLoS Pathog*. 3(10):1486-1501. doi:10.1371/journal.ppat.0030158

Schneider, I. (1972). Cell lines derived from late embryonic stages of *Drosophila melanogaster*. *J. Embryol. Exp. Morphol*. 27, 353-365.

Siebel C., Lendahl U. (2017). Notch Signaling in Development, Tissue Homeostasis, and Disease. *Physiol Rev*. 97(4):1235-1294. doi:10.1152/physrev.00005.2017

Sinenko, S.A., Hung, T., Moroz, T., Tran, Q.M., Sidhu, S., Cheney, M.D., Speck, N.A., Banerjee, U. (2010). Genetic manipulation of AML1-ETO-induced expansion of hematopoietic precursors in a *Drosophila* model. *Blood* 116(22):4612-4620. doi:10.1182/blood-2010-03-276998

Sinenko, S.A., Shim, J., Banerjee, U. (2011). Oxidative stress in the haematopoietic niche regulates the cellular immune response in *Drosophila*. *EMBO Rep*. 13: 83–89. doi:10.1038/embor.2011.223

Small, C., Ramroop, J., Otazo, M., Huang, L.H., Saleque, S., Govind, S. (2014). An unexpected link between Notch signaling and ROS in restricting the differentiation of hematopoietic progenitors in *Drosophila*. *Genetics* 197(2):471-483. doi: 10.1534/genetics

Smith, D.B., Johnson, K.S. (1988). Single-step purification of polypeptides expressed in *Escherichia coli* as fusions with glutathione S-transferase. *Gene* 67(1):31-40. doi: 10.1016/0378-1199(88)90005-4

Sorrentino, R.P., Carton, Y., Govind, S. (2002). Cellular immune response to parasite infection in the *Drosophila* lymph gland is developmentally regulated. *Dev. Biol. 243*(1), 65–80. https://doi.org/10.1006/dbio.2001.0542

844 Spitzer, M., Wildenhain, J., Rappsilber, J., Tyers, M. (2014). BoxPlotR: a web tool for
845 generation of box plots. *Nature methods 11*(2), 121–122. doi: 10.1038/nmeth.2811
846 Stofanko, M., Kwon, S.Y., Badenhorst, P. (2010). Lineage tracing of lamellocytes
847 demonstrates *Drosophila* macrophage plasticity. *PLoS One* 5, e14051.
848 doi:10.1371/journal.pone.0014051.
849 Tattikota, S.G., Cho, B., Liu, Y., Hu, Y., Barrera, V., Steinbaugh, M.J., Yoon, S.-H.,
850 Comjean, A., Li, F., Dervis, F., Hung, R.-J., *et al.* (2020). A single-cell survey of
851 *Drosophila* blood. *Elife* 9. doi:10.7554/eLife.54818
852 Terriente-Felix, A., Li, J., Collins, S., Mulligan, A., Reekie, I., Bernard, F., Krejci, A., Bray,
853 S. (2013). Notch cooperates with Lozenge/Runx to lock haemocytes into a differentiation
854 programme. *Development* 140:926–937. doi:10.1242/dev.086785
855 Vanha-Aho, L. M., Anderl, I., Vesala, L., Hultmark, D., Valanne, S., Rämet, M. (2015). Edin
856 expression in the fat body is required in the defense against parasitic wasps in *Drosophila*
857 *melanogaster*. *PLoS Pathog*. 11(5):e1004895. doi:10.1371/journal.ppat.1004895
858 Voolstra, O., Beck, K., Oberegelsbacher, C., Pfannstiel, J., Huber, A. (2010). Light-dependent
859 phosphorylation of the *Drosophila* transient receptor potential ion channel. *J Biol Chem.*
860 285, 14275–14284. doi:10.1074/jbc.M110.102053
861 Weiss, I., Ruther, J., Stöckl, J. (2015). Species specificity of the putative male antennal
862 aphrodisiac pheromone in *Leptopilina heterotoma*, *Leptopilina boulardi* and *Leptopilina*
863 *victoriae*. *Biomed Res Int*. 202965. doi: 10.1155/2015/202965.
864 Wilson, J.J., Kovall, R.A. (2006). Crystal structure of the CSL-Notch-Mastermind ternary
865 complex bound to DNA. *Cell* 124(5):985-996. doi:10.1016/j.cell.2006.01.035
866 Wolf, D., Smylla, T.K., Reichmuth, J., Hoffmeister, P., Kober, L., Zimmermann, M.,
867 Turkiewicz, A., Borggrefe, T., Nagel, A.C., Oswald, F., *et al.* (2019). Nucleo-cytoplasmic
868 shuttling of *Drosophila* Hairless/Su(H) heterodimer as a means of regulating Notch
869 dependent transcription. *Biochim Biophys Acta Mol Cell Res*. 1866(10):1520-1532. doi:
870 10.1016/j.bbamcr.2019.07.008
871 Xue, Y., Liu, Z., Cao, J., Ma, Q., Gao, X., Wang, Q., Jin, C., Zhou, Y., Wen, L., Ren, J.
872 (2011). GPS 2.1: enhanced prediction of kinase-specific phosphorylation sites with an
873 algorithm of motif length selection. *Protein Eng Des Sel* 24(3):255-260. doi:
874 10.1093/protein/gzq094
875 Yashiro-Ohtani, Y., He, Y., Ohtani, T., Jones, M.E., Shestova, O., Xu, L., Fang, T. C.,
876 Chiang, M.Y., Intlekofer, A.M., Blacklow, S.C., *et al.* (2009). Pre-TCR signaling

877 inactivates Notch1 transcription by antagonizing E2A. *Genes Dev*. 23(14):1665-1676.
878 doi:10.1101/gad.1793709.
879 Yui, M.A., Rothenberg, E.V. (2014). Developmental gene networks: a triathlon on the course
880 to T cell identity. *Nat Rev Immunol*. 2014;14(8):529-545. doi:10.1038/nri3702

881 **Figures**

882 **Figure 1**

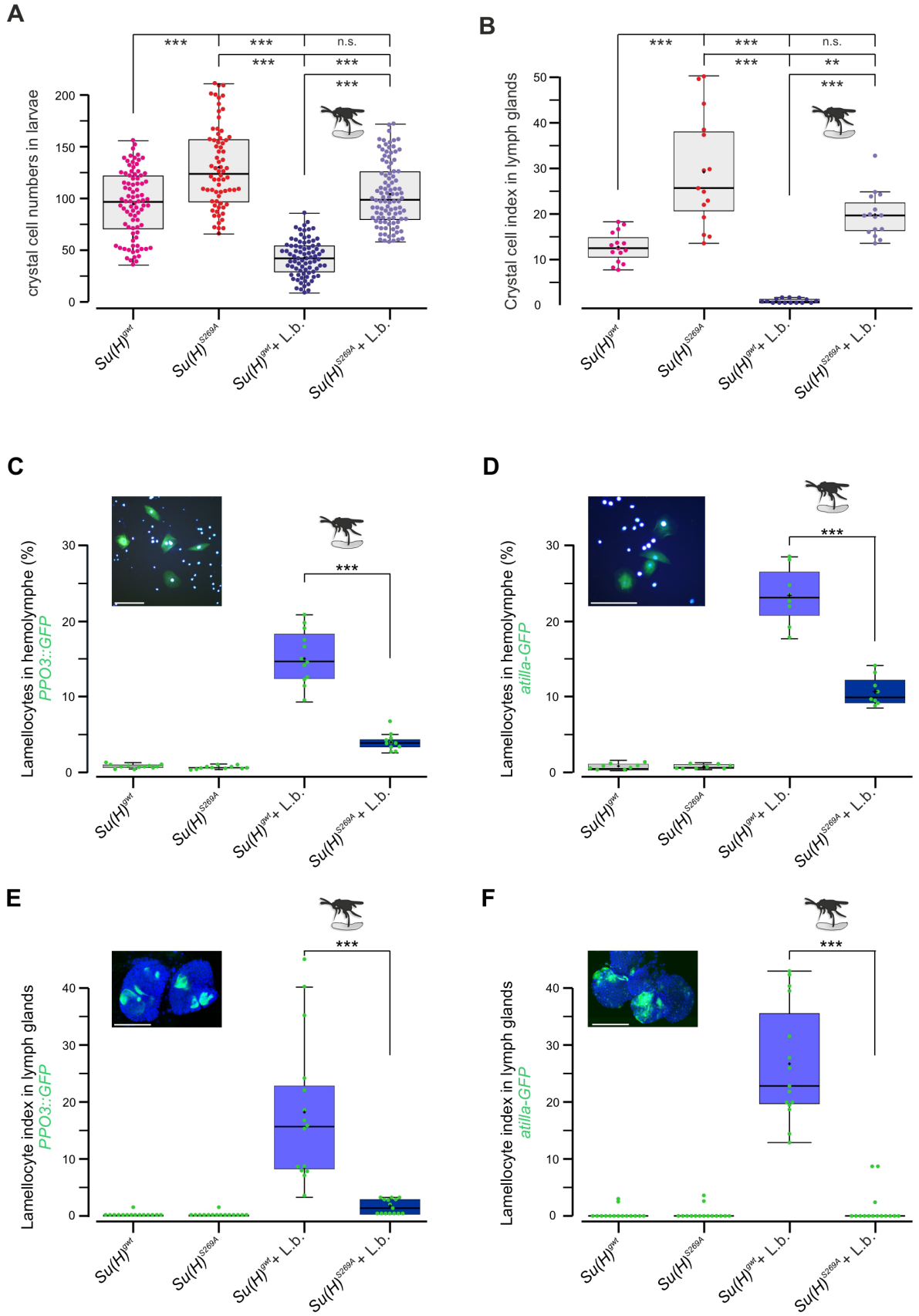

883

884

885 ***Figure 1 Su(H)^{S269A} mutants are compromised in their response to parasitoid wasp***
886 ***infestation***
887 (**A**) Quantification of melanized crystal cells from the last two segments of *Su(H)^{gwt}* and
888 *Su(H)^{S269A}* larvae with and without wasp infestation as indicated. In the control, wasp
889 parasitism causes crystal cell numbers to drop to a level of about 50%, whereas in *Su(H)^{S269A}*
890 mutants the number settles at the un-infested *Su(H)^{gwt}* level. Each dot represents one analysed
891 larva (n=70-100). (**B**) Crystal cell index in larval lymph glands is given as ratio of Hnt-
892 positive crystal cells per 1° lobe relative to the size of the lobe. Each point represents one
893 analysed lobus (n=15). Statistical analyses with ANOVA for multiple comparisons, using
894 Tukey-Kramer approach with *** $p \leq 0.001$, ns (not significant $p > 0.05$).
895 (**C-F**) Quantification of larval lamellocytes in the circulating hemolymph (C,D) or in lymph
896 glands (E,F) before and after wasp infestation in *Su(H)^{gwt}* versus *Su(H)^{S269A}*. Lamellocytes
897 were marked with either *PPO3-Gal4::UAS*-GFP (C,E) or *atilla*-GFP (D,F) as indicated.
898 (C,D) The fraction of GFP-labelled lamellocytes of the total number of DAPI-labelled blood
899 cells isolated from hemolymph is given; each dot represents ten pooled larvae. Representative
900 image of labelled control hemolymph is shown above (DAPI-labelled nuclei in light blue,
901 GFP in green). Scale bars 50 µm.
902 (E,F) Lamellocyte index is given as number of GFP-labelled lamellocytes per area in the 1°
903 lobe of the lymph gland. Each dot represents the lamellocyte index of one lobus (n=12).
904 Representative *Su(H)^{gwt}* lymph glands after infestation are shown above, co-stained for
905 nuclear Pzg (in blue). Scale bars 100 µm. Statistical analyses with ANOVA using Dunnet's
906 approach relative to *Su(H)^{gwt}* control; only significant differences are indicated (*** $p \leq 0.001$).

907 **Figure 2**

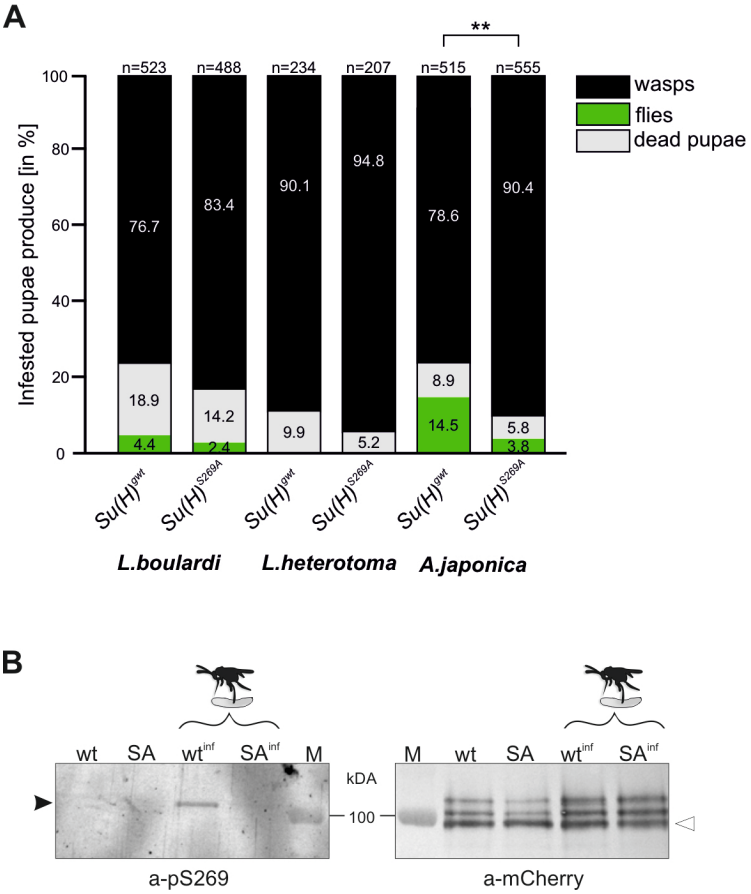

908

909

910 ***Figure 2 Resistance to wasp infestation and phosphorylation at S269***

911 **(A)** Resistance of *Su(H)*^{gwt} and *Su(H)*^{S269A} to the infestation with parasitic wasp strains *L.*
912 *boulardi* and *L. heterotoma* (both family Figitidae) and *A. japonica* (family Braconidae), as
913 indicated. Numbers of eclosed flies versus wasps as well as of dead pupae are presented in
914 relation to the total of infested pupae. At least three independent experiments were performed,
915 n=number of infested pupae. Statistically significant difference determined by Student's T-
916 test is indicated with **$p \leq 0.01$.

917 **(B)** Su(H) is phosphorylated at Serine 269 upon parasitoid wasp infestation. Protein extracts
918 from *Su(H)*$^{gwt\text{-}mCh}$ (wt) and *Su(H)*$^{S269A\text{-}mCh}$ (SA) larvae, respectively, infested (wt^{inf}, SA^{inf}) or
919 not with *L. boulardi*, were isolated by RFP-Trap precipitation and probed in Western blots.
920 The α-pS269 antiserum specifically detects wild type Su(H) protein only in wasp infested
921 larvae (arrowhead), but not the Su(H)^{S269A} isoform. The blot on the right serves as loading
922 control, probed with α-mCherry antibodies, revealing the typical Su(H) protein pattern in all
923 lanes; the lowest band presumably stems from degradation (open arrowhead). M, prestained
924 protein ladder, protein size is given in kDa.

925 **Figure 3**

926

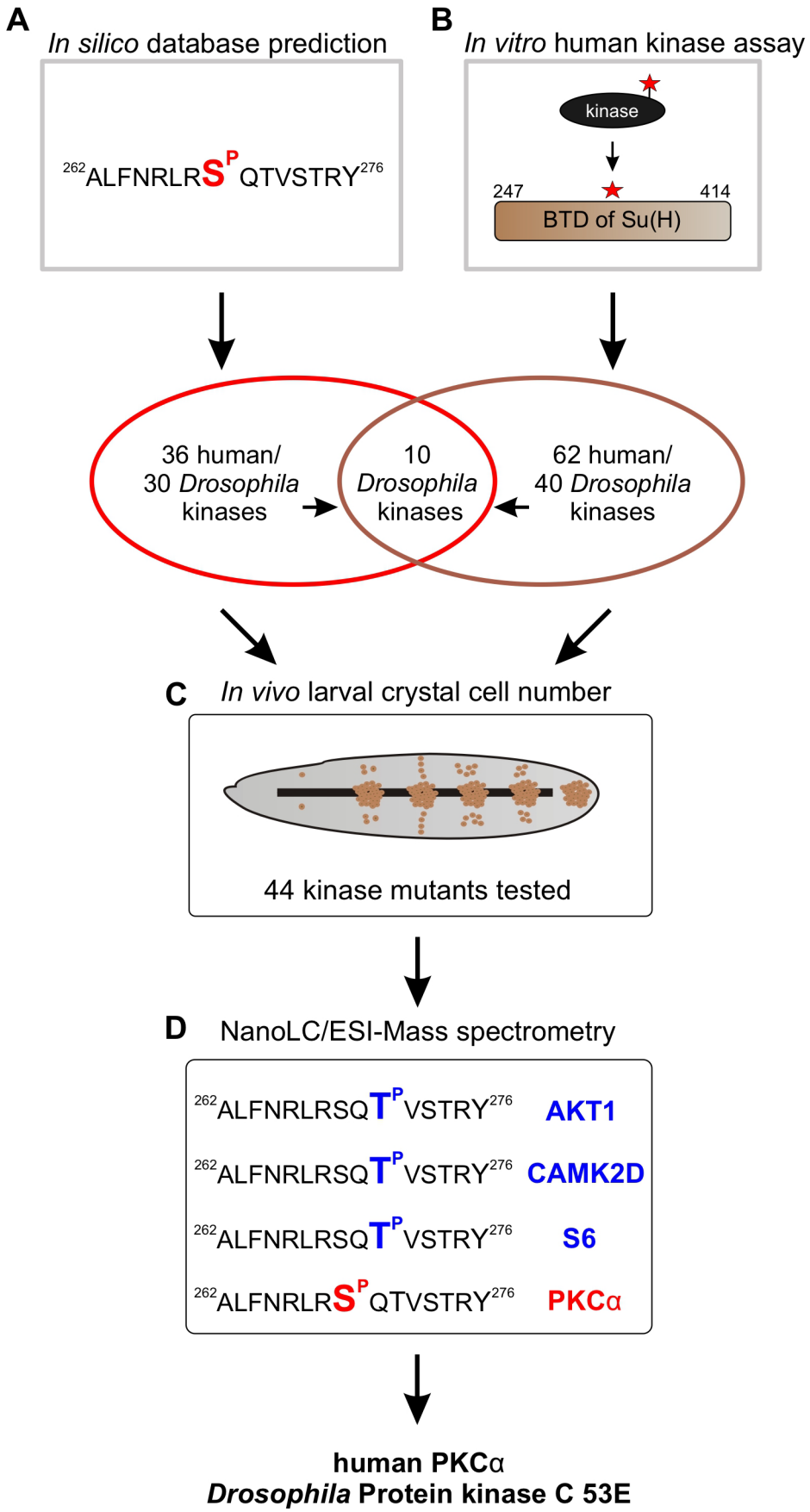

927

928 ***Figure 3 Pipeline of screening procedures for kinase candidates triggering phosphorylation***
929 ***at Su(H)^{S269}***
930 (**A**) *In silico* screening of database(s) predicting kinase recognition motif in Su(H)^{S269}; see
931 supplement Table 1. (**B**) *In vitro* assay screening 245 human Ser/Thr kinases for their ability
932 to phosphorylate the BTD domain of Su(H) ; see supplement Table 2. **(C)** *In vivo* screen of 44
933 different *Drosophila* kinase mutants for crystal cell occurrence in third instar larvae; see
934 supplement Table 4. **(D)** NanoLC/ESI mass spectrometry with active human kinases
935 monitoring their ability to phosphorylate the given Su(H) peptide. PKCα phosphorylates
936 S269, whereas AKT1, CAMK2D and S6 kinase prefer T271. Spectra are shown in figure
937 supplement 1.

938 **Figure 4**

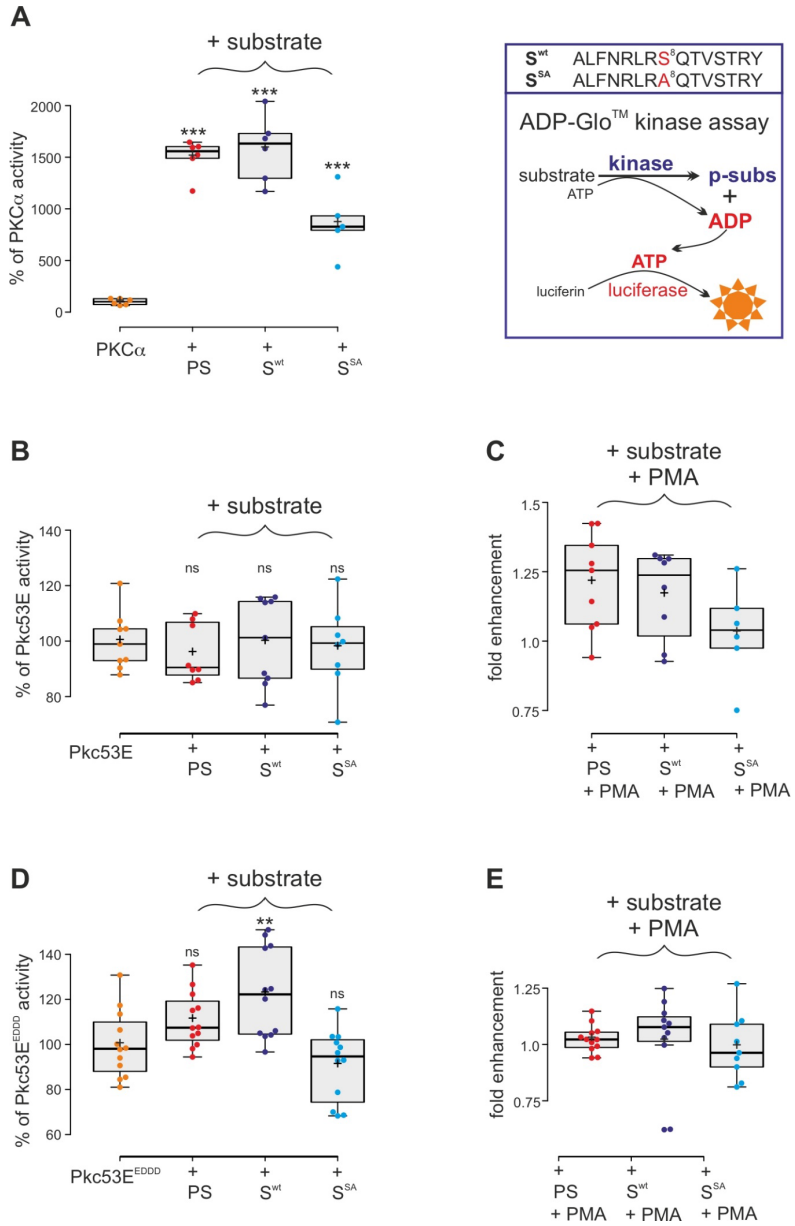

939

940

941 ***Figure 4 Kinase assays using activated PKCα and Drosophila Pkc53E variants***

942 (**A**) Right, schema of ADP-Glo™ assay to quantify kinase activity. The wild type (S^{wt}) and
943 mutant (S^{SA}) Su(H) peptides 262-276 offered as specific kinase substrates are indicated
944 above. Left, commercially available, active PKCα very efficiently phosphorylates the pseudo-
945 substrate PS and the Su(H) S^{wt} peptides, but less efficiently the S^{SA} mutant peptide. Activity is
946 given as percentage of the auto-active kinase without substrate. (**B**) Bacterially expressed
947 Pkc53E has no activity on any of the offered substrates PS, S^{wt} or S^{SA}. (**C**) PMA raised
948 Pkc53E activity to nearly 125% for PS and S^{wt} but not for S^{SA}. (**D**) Activated $Pkc53^{EDDD}$

949 triggers phosphorylation of PS and S^{wt} but not of S^{SA}. (**E**) Addition of PMA does not change
950 $Pkc53^{EDDD}$ activity.
951 **Figure 5**

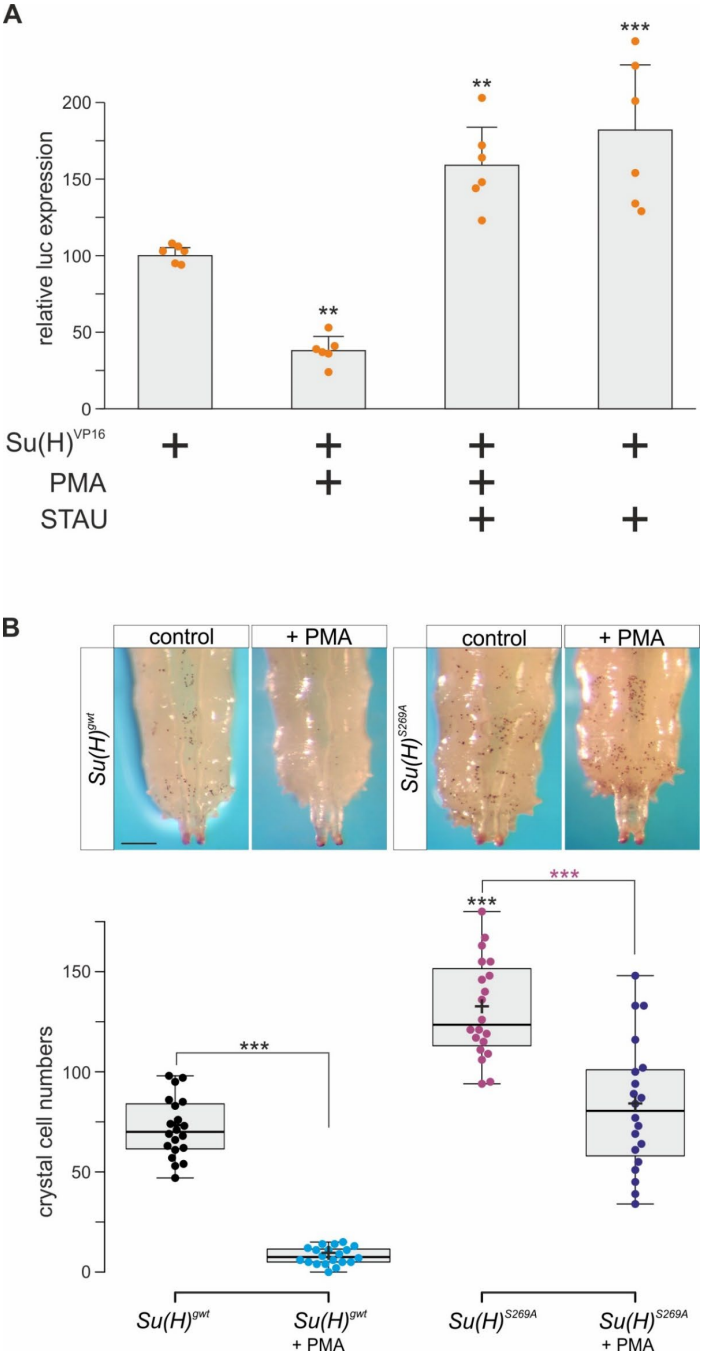

952
953
954 ***Figure 5 PMA induced activation of Pkc53E inhibits Su(H) transcriptional activity in vitro***
955 ***and crystal cell formation in vivo***
956 **(A)** 2xMyc-Su(H)-VP16 $(SuH)^{VP16}$), transfected into *RBPj*^{ko} HeLa cells, activates expression
957 of a luciferase-reporter gene independent of Notch activity. Luciferase activity is given
958 relative to the value of the reporter construct alone; the Su(H)-VP16 value is taken as 100%.

959 Addition of PMA reduces Su(H)-VP16 dependent transcriptional activity to about 40%,
960 which is reversed by the inhibitor Staurosporine (STAU). STAU itself increases Su(H)-VP16
961 activity nearly twofold. Six independent experiments were performed. Bars show the mean,
962 error bars indicate standard deviation. Statistical analysis was performed with a two-way
963 ANOVA for multiple comparisons, Dunnet's test with *** $p \leq 0.001$, ** $p \leq 0.01$ relative to
964 Su(H)-VP16 alone.
965 **(B)** Number of melanized larval crystal cells determined in the last two segments of larvae fed
966 with normal fly food, or with fly food plus PMA (n=20). Note strong drop of crystal cell
967 numbers in the $Su(H)^{gwt}$ control fed with PMA, in contrast to the $Su(H)^{S269A}$ mutant larvae,
968 where numbers drop to only control level. Representative animals are shown above; scale bar
969 250 µm. Statistical analysis by two-way ANOVA for multiple comparisons, Tukey-Kramer
970 approach (*** $p \leq 0.001$), significant differences are colour coded.

971 **Figure 6**

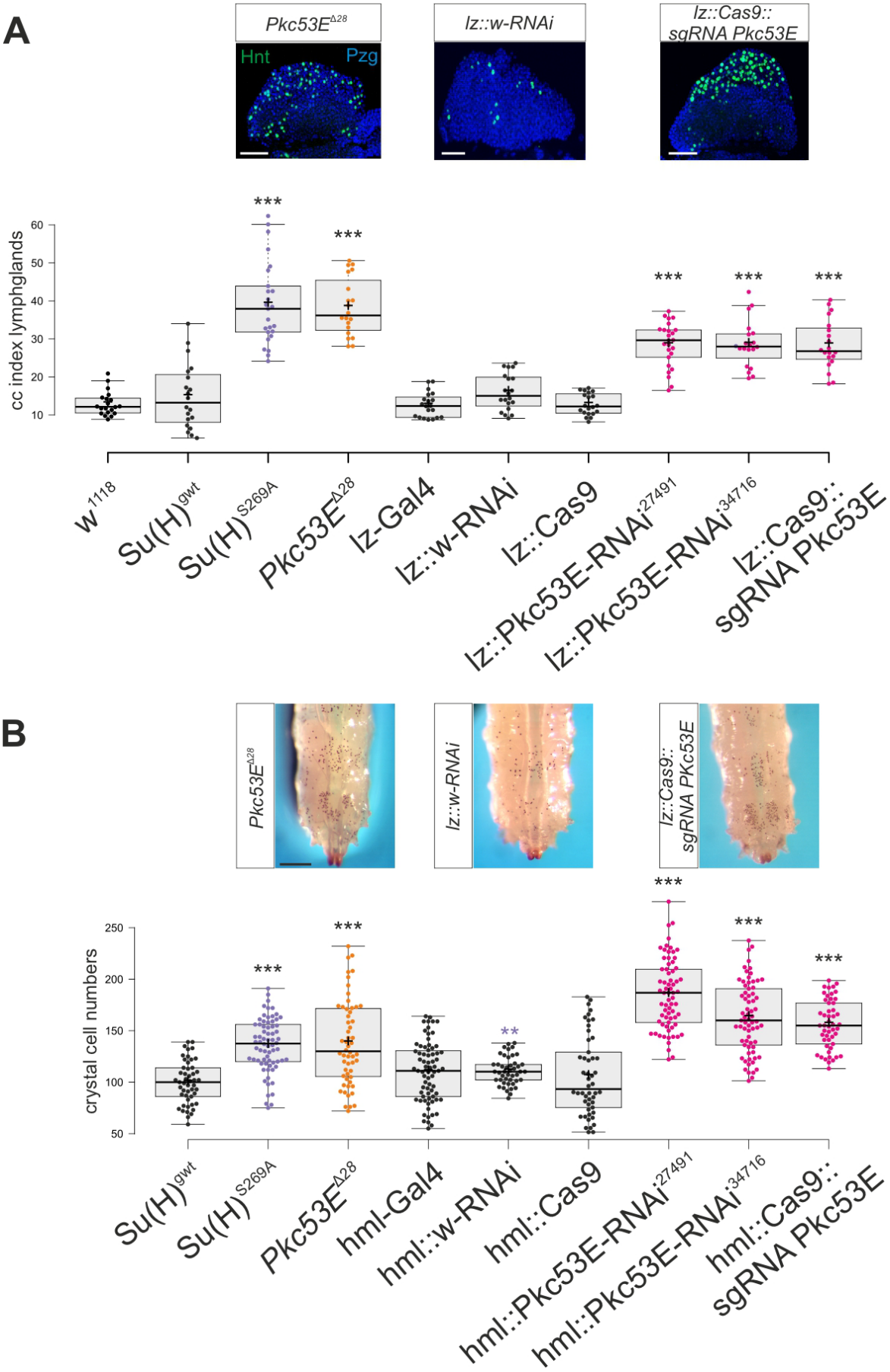

972

973 ***Figure 6 Loss of Pkc53E causes a gain of crystal cell number***

974 Depletion of *Pkc53E* activity in the *Pkc53E*$^{\Delta 28}$ mutant or after knock down by *Pkc53E*-RNAi
975 or sg*Pkc53E* with the help of the Gal4/UAS system using *lz*-Gal4 (A) or *hml*-Gal4 (B).
976 Controls as indicated. **(A)** Crystal cell index in lymph glands; each dot represents the value of
977 an analysed lobus (n= 20-25). Representative examples of *Pkc53E*$^{\Delta 28}$, *lz*::*Pkc53-RNAi* and
978 *lz*::*Cas9 sgPkc53E* are shown above. Crystal cells are labelled with Hnt (green), the lobe is
979 stained with α-Pzg (blue). Scale bar 50 µm.
980 **(B)** Melanized crystal cells enumerated from the last two segments of larvae with the given
981 genotype (n=45-70). Representative examples of the evaluated last segments of *Pkc53E*$^{\Delta 28}$,
982 *lz*::*Pkc53*-RNAi and *lz*::*Cas9 sgPkc53E* are shown above. Scale bar 250 µm. ANOVA for
983 multiple comparisons, Dunnet's approach relative to controls with *** $p \leq 0.001$. Note that
984 there were no significant differences between any of the controls shown in black.

Figure 7

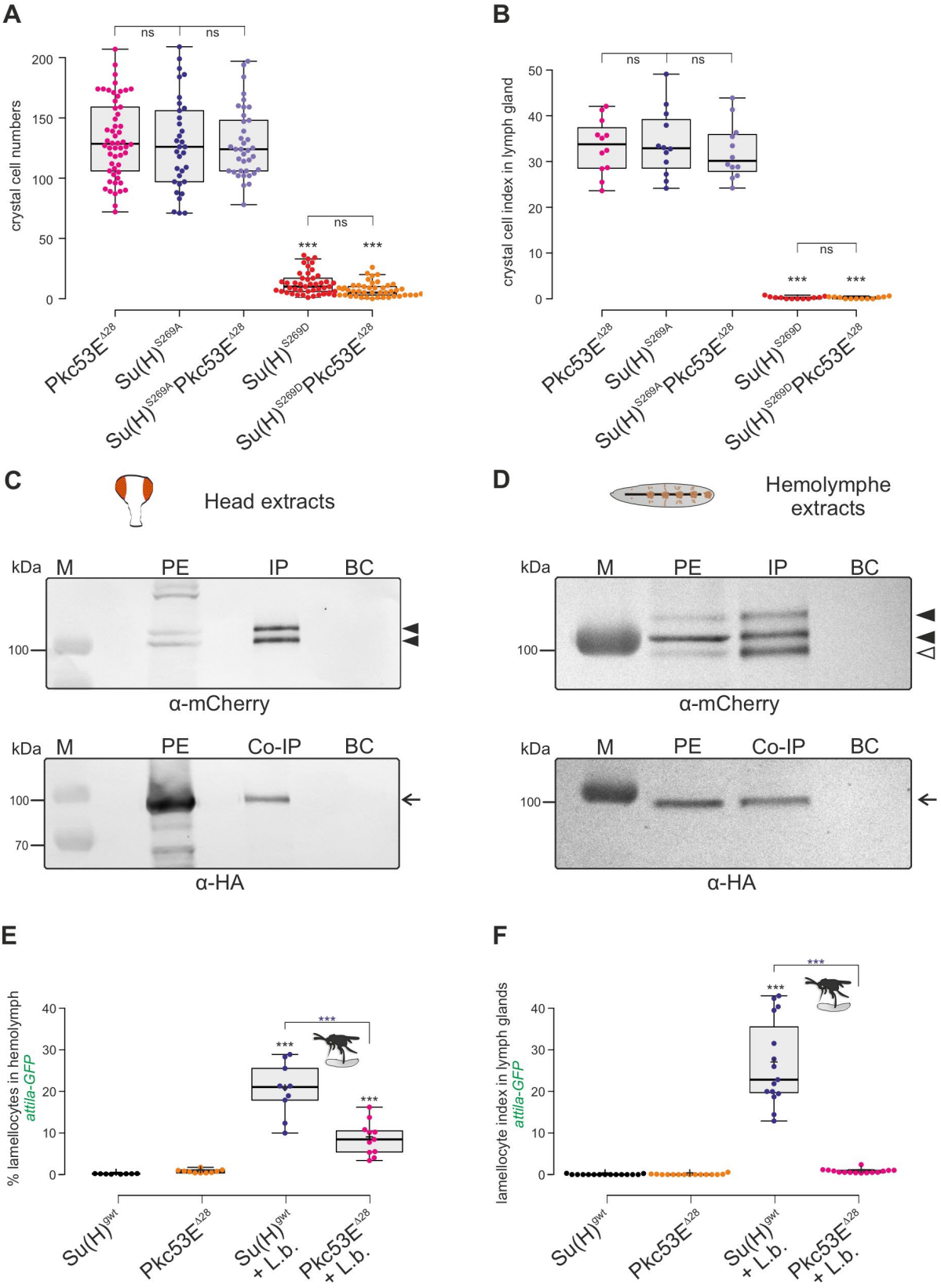
A
crystal cell numbers
ns
ns
ns
***
***
Pkc53E^Δ28
Su(H)^S269A
Su(H)^S269A Pkc53E^Δ28
Su(H)^S269D
Su(H)^S269D Pkc53E^Δ28
B
crystal cell index in lymph gland
C
Head extracts
kDa
M
PE
IP
BC
100
α-mCherry
Co-IP
70
α-HA
D
Hemolymphe extracts
E
% lamellocytes in hemolymph
attila-GFP
Su(H)^gwt
Pkc53E^Δ28
Su(H)^gwt + L.b.
Pkc53E^Δ28 + L.b.
F
lamellocyte index in lymph glands

989 ***Figure 7 Pkc53E interacts with Su(H) and is immune compromised***

990 **(A)** Larval crystal cell number and **(B)** crystal cell indices in lymph glands were determined
991 in the given genotypes. Each dot represents one analysed larva (n=33-70) in (A) or lymph
992 gland lobus (n=12) in (B). ANOVA for multiple comparisons, Tukey-Kramer's approach
993 relative to controls with *** $p \leq 0.001$; $p > 0.05$ ns (not significant).

994 (**C,D**) Co-immuno-precipitation of $Pkc53E^{HA}$ with $Su(H)^{gwt\text{-}mCh}$ protein. RFP-Trap IP was
995 performed on protein extracts from 400 heads (C) and 25 third instar larvae (D), respectively.
996 UAS-Pkc53E-HA expression was induced with *Gmr*-Gal4 in the head or *hml*-Gal in the
997 hemolymph. Endogenous mCherry-tagged Su(H) was trapped and detected with α-mCherry
998 antibodies (black arrowheads). The lowest band from the hemolymph is presumably a
999 degradation product (open arrowhead in (D)). HA-tagged Pkc53E was specifically co-
1000 precipitated as detected with anti-HA antibodies (arrow). 10% of the protein extract (PE) used
1001 for the IP-Trap was loaded for comparison. BC describes the Trap with only agarose beads as
1002 a control. M, pre-stained protein ladder; protein size is given in kDa.

1003 **(E,F)** Quantification of lamellocytes labelled with the *atilla*-GFP reporter in the circulating
1004 hemolymph (E) or in the lymph glands (F), in un-infested conditions or upon wasp infestation
1005 as indicated. **(E)** Fraction of GFP-positive lamellocytes relative to the total of DAPI-stained
1006 hemocytes in the pooled hemolymph from ten larvae. Each dot represents one larval pool
1007 (n=12 experiments). **(F)** Lamellocyte index, i.e. number of GFP-labelled cells relative to the
1008 size of the lymph gland (n=15). Statistical analysis by ANOVA multiple comparisons with
1009 Tukey-Kramer's test; *** $p \leq 0.001$.

Additional information

Funding

This work was supported by a grant of the German Science Foundation DFG to ACN (NA 427/5-1) and by the University of Hohenheim. The funders had no role in study design, data collection and interpretation, or the decision to submit the work for publication.

Author contributions

Sebastian Deichsel, Data curation, Formal analysis, Methodology, Investigation, Resources, Writing—review and editing, Validation, Visualization; Lisa Frankenreiter, Formal analysis, Methodology, Investigation, Resources, Writing—review and editing, Validation; Johannes Fechner, Formal analysis, Methodology, Investigation, Resources, Writing—review and editing, Validation; Bernd M. Gahr, Data curation, Methodology, Investigation, Resources, Writing—review and editing, Visualization; Mirjam Zimmermann, Formal analysis, Investigation, Resources, Writing—review and editing; Helena Mastel, Investigation, Writing—review and editing; Irina Preis, Investigation, Writing—review and editing; Anette Preiss, Formal analysis, Writing—original draft, Writing—review and editing, Visualization; Anja C. Nagel, Conceptualization, Data curation, Formal analysis, Methodology, Writing—original draft, Writing—review and editing, Validation, Visualization, Supervision, Funding acquisition, Project administration.

Author ORCIDs

Anette Preiss, https://orcid.org/0000-0002-6410-1586

Anja C. Nagel, https://orcid.org/0000-0002-2733-3249

Supplemental Materials

Figures Supplement

Figure 2 - figure supplement 1

The α-pS269 antiserum detects the phospho-mimetic Su(H) variant in vitro

Figure 3D – figure supplement 1

MS/MS spectra of the phosphorylated Su(H) peptide

Figure 4 – figure supplement 1

Conservation of Pkc53E and generation of an activated Pkc53E^{EDDD} isoform

1044 **Figure 6 – figure supplement 1**

1045 *The Pkc53E$^{\Delta 28}$ allele is a null mutant*

1046

1047 **Tables Supplement**

1048 **Figure 3 – supplement Table 1**

1049 List of kinases predicted to recognize S269 in Su(H) as substrate *in silico*

1050 **Figure 3 – supplement Table 2**

1051 List of kinases accepting the BTD domain of Su(H) as substrate *in vitro*

1052 **Figure 3 – supplement Table 3**

1053 Fly strains used for the larval crystal cell screen

1054 **Figure 3 – supplement Table 4**

1055 Larval crystal cell screen

1056

1057 **Supplemental Tables, Materials and Methods**

1058 **S1 Table** Key resources

1059 **S2 Table** Oligonucleotides